

# Benchmarking the Ising Universality Class in $3 \leq d < 4$ dimensions

C. Bonanno<sup>1\*</sup>, A. Cappelli<sup>1</sup>, M. Kompaniets<sup>2,3</sup>, S. Okuda<sup>4</sup>, K. J. Wiese<sup>5</sup>

**1** INFN, Sezione di Firenze, Via G. Sansone 1, 50019 Sesto Fiorentino (FI), Italy

**2** Saint Petersburg State University, 7/9 Universitetskaya Embankment, St. Petersburg, 199034, Russia

**3** Bogoliubov Laboratory of Theoretical Physics, JINR, 6 Joliot-Curie, Dubna, 141980, Russia

**4** Department of Physics, Rikkyo University Toshima, Tokyo 171-8501, Japan

**5** Laboratoire de Physique de l'École Normale Supérieure, Université PSL, CNRS, Sorbonne Université, Université Paris-Diderot, Sorbonne Paris Cité, 24 rue Lhomond, 75005 Paris, France

\*claudio.bonanno@fi.infn.it

March 9, 2023

## 1 Abstract

**2** The Ising critical exponents  $\eta$ ,  $\nu$  and  $\omega$  are determined up to one-per-thousand relative error in the whole range of dimensions  $3 \leq d < 4$ , using numerical conformal-  
**3** bootstrap techniques. A detailed comparison is made with results by the resummed  
**4** epsilon expansion in varying dimension, the analytic bootstrap, Monte Carlo and non-  
**5** perturbative renormalization-group methods, finding very good overall agreement.  
**6** Precise conformal field theory data of scaling dimensions and structure constants are  
**7** obtained as functions of dimension, improving on earlier findings, and providing bench-  
**8** marks in  $3 \leq d < 4$ .  
**9**

10

## 11 Contents

12	<b>1 Introduction</b>	<b>2</b>
13	<b>2 Conformal bootstrap in non-integer dimension</b>	<b>3</b>
14	2.1 Summary of numerical methods	3
15	2.2 Analysis of conformal dimensions of the three leading fields for $4 > d \geq 3$	6
16	<b>3 Comparison with the epsilon expansion in <math>4 &gt; d \geq 3</math></b>	<b>9</b>
17	3.1 Warm-up analysis of the anomalous dimensions $\gamma_\sigma$	9
18	3.2 Bootstrap data versus resummed perturbative results	13
19	<b>4 Structure constants and scaling dimensions of higher fields</b>	<b>22</b>
20	4.1 Structure constants in $4 > d \geq 3$	22
21	4.2 Higher fields $T'$ and $C$	25
22	4.3 Subleading fields $\epsilon''$ and $C'$	27

23	<b>5 Conclusions</b>	<b>29</b>
24	<b>A Orthogonal polynomial regression</b>	<b>31</b>
25	<b>B Resummation of perturbative series</b>	<b>32</b>
26	B.1 Toy model example	32
27	B.2 Details on the resummation method	35
28	<b>References</b>	<b>37</b>

---

29  
30

## 31 1 Introduction

32 Many approaches to critical phenomena obtain results in continuous space dimension, although  
33 physically relevant dimensions are integer. Most notable is the perturbative renormalization group  
34 in  $d = 4 - \epsilon$  dimensions [1–4]. This is not merely a technical issue: quantities as functions of real  
35  $d$  can clarify features that are harder to see at discrete values. E.g., one can follow the topology  
36 of the renormalization-group (RG) flow as a function of dimension and find instances where the  
37 universality class changes at non-integer values. This proved particularly useful for systems with  
38 long-range interactions [5–7] or disorder [8–13].

39 The recent very precise numerical conformal bootstrap [14–16] has been formulated in continuous  
40 dimension [17, 18], in particular for the Ising model in its whole range  $4 > d \geq 2$  [19–21]. The  
41 interest lies in understanding how the strongly interacting Ising conformal field theory connects  
42 to a free scalar in  $d = 4$  and to the integrable fully-solvable model in  $d = 2$  [22, 23]. Analytic  
43 bootstrap approaches which use the dimension as a tunable parameter were also developed [24–32].  
44 Initially, the non-unitarity of the theory in non-integer dimensions [33] was thought to hamper the  
45 numerical methods involving positive quantities. These concerns have been overcome by *de facto*  
46 never observing problems for the quantities of interest, as explained later.

47 In this paper, we extend the numerical approach of Ref. [20] using a single correlator, the  
48 SDPB [34] routine for determining the unitarity domain, and the Extremal Functional Method [35,  
49 36] for solving the bootstrap equations. We obtain improved results for the scaling dimensions in  
50  $4 > d \geq 3$  by a denser scanning of the unitary region near the Ising point, i.e., the kink. The latter  
51 gets parametrically sharper as  $d$  approaches 4, allowing for its better identification. The conformal  
52 spectrum in dimensions  $4 > d \geq 2.6$  has also been obtained in Ref. [21] via the advanced *navigator*  
53 bootstrap technique [37]. We use these very precise results in combination with ours to obtain a  
54 consistent description of the low-lying spectrum.

55 The achieved precision allows us to perform a detailed comparison with state-of-the-art epsilon  
56 expansion in two regimes: for  $d$  close to 4, the series is directly compared to bootstrap data,  
57 using the necessary finer scale for the latter; for intermediate values between 4 and 3 (included),  
58 the divergent perturbative series is resummed using well-established methods involving the Borel  
59 transform [38–41].

60 The analysis is done on the dimensions of the conformal fields  $\sigma, \epsilon, \epsilon'$ , corresponding to spin,  
61 energy and subleading energy. They determine the critical exponents  $\eta, \nu, \omega$ . The precision of our

bootstrap data is summarized by the (mostly)  $d$ -independent value of the relative error  $\text{Err}(\gamma)/\gamma = O(10^{-3})$  for the anomalous dimensions  $\gamma$  of the conformal fields  $\sigma$  and  $\epsilon$ . As the anomalous dimensions are very small for  $d \approx 4$ , the precision for the conformal dimensions  $\Delta_\sigma, \Delta_\epsilon$  is even higher in this region. Regarding the subleading energy, the relative error  $\text{Err}(\Delta_{\epsilon'})/\Delta_{\epsilon'}$  stays at three digits, as explained later. Some of the structure constants are determined with a higher  $O(10^{-4})$  accuracy.

We compare our data with recent results of the analytic bootstrap [27–32], Monte Carlo simulations [42–44] and the non-perturbative RG [45, 46]. We find that the data by all methods agree very well. This is rather rewarding given the achieved precision. Besides confirming the high quality of conformal-bootstrap results, our analysis provides a reference point for further analytic and numerical methods aiming at exploring critical phenomena in varying dimensions.

The outline of this paper is the following. In Sec. 2 we summarize our bootstrap protocol [20] and present the results for the three main conformal dimensions mentioned above, together with their polynomial fits as a function of dimension and the estimation of errors. In Sec. 3 we briefly recall the properties of the epsilon expansion and resummation techniques. We then compare its predictions with our bootstrap data and the results by other methods, and authors. A detailed analysis of all issues is presented. In Sec. 4, we report the numerical bootstrap data for scaling dimensions of structure constants and other conformal fields, and compare them to the existing epsilon expansion. In the conclusions in Sec. 5 we discuss open questions.

## 2 Conformal bootstrap in non-integer dimension

The aim of this section is to summarize our procedure for deriving conformal data of scaling dimensions and structure constants, as a function of the space-time dimension  $4 > d \geq 2$ . We first discuss the conformal dimensions of three main fields  $\mathcal{O} = \sigma, \epsilon, \epsilon'$ . Our goal is to provide a polynomial description of  $\Delta_{\mathcal{O}}$  as a function of  $y = 4 - d$ , by performing a *best fit* of the data obtained at several values of  $d^1$ . Our results are finally compared to those obtained from the resummed epsilon expansion in Section 3.

### 2.1 Summary of numerical methods

The conformal dimensions and structure constants of the critical Ising model as a function of  $d$  are computed in the setup of Ref. [20], which we shortly summarize for the reader's convenience. We consider a single 4-point correlator  $\langle \sigma(x_1)\sigma(x_2)\sigma(x_3)\sigma(x_4) \rangle$ , where  $\sigma(x)$  is the primary scalar field with lowest dimension, denoted  $\Delta_\sigma$ . We truncate the functional bootstrap equation to 190 components<sup>2</sup>. The unitarity condition for this equation is determined through the SDPB algorithm [34], leading to a bound in the  $(\Delta_\sigma, \Delta_\epsilon)$  plane; next, the Extremal Functional Method (EFM) [35, 36] is used to solve the equations on this boundary. We use the generalization of these numerical methods to non-integer dimensions developed in Ref. [20], and detailed in its Appendix A.

Our 1-correlator numerical bootstrap approach has been surpassed by more recent implementations [16, 19, 21, 47, 48], but we find it convenient for determining the low-lying spectrum with

<sup>1</sup>Note that  $\epsilon$  is the energy field, the next-to-lowest scalar primary field, not to be confused with the deviation from four dimensions denoted by  $y$ .

<sup>2</sup>This corresponds to the standard bootstrap parameter  $\Lambda = 18$ , which counts the number of derivatives in the approximation of the functional basis.

99 modest computing resources. The complete determination of the conformal data for one value of  $d$   
 100 requires about 20 hours on 256 cores, corresponding to 5000 core hours. This simple setting allows  
 101 us to evaluate the spectrum for various dimensions  $d$ .

102 The first crucial step is to locate the Ising critical point in parameter space. To this end, we  
 103 adopt the twofold strategy of Ref. [20], consisting in searching the kink on the unitarity boundary  
 104 in the  $(\Delta_\sigma, \Delta_\epsilon)$  plane and, at the same time, minimizing the central charge  $c$  [15]. This procedure  
 105 allow us to determine for each value of  $d$  an interval of values for  $\Delta_\sigma, \Delta_\epsilon$  and  $c$ , that we take as the  
 106 Ising conformal theory, accompanied by an estimate of the uncertainty.

107 This procedure is displayed in Fig. 1, where we show the identification of the Ising point for  
 108  $d = 3, 3.25, 3.5$  and  $3.75$ . The gray area in the plots indicates the chosen errors for  $\Delta_\sigma, \Delta_\epsilon$  and  
 109  $c$ , which are roughly determined by the mismatch between the positions of the minimum and the  
 110 kink. As a conservative choice, we consider an interval of four data points for each value of  $d$ .

111 The precision is greater than in Ref. [20], because we perform a finer scan of the  $\Delta_\sigma$  values  
 112 around the kink. We observe that the kink and the minimum get sharper for  $d \rightarrow 4$ , as shown by  
 113 the four pairs of plots drawn on the same scale in Fig. 1; this is convenient in our approach, since  
 114 it leads to an increased precision when anomalous dimensions are smaller. In Fig. 2, we show the  
 115 point  $d = 3.875$ , not considered in the earlier work. It is necessary for studying the region of  $d \rightarrow 4$ .  
 116 Here the curves are so steep that magnified scales are needed.

117 Once the Ising point is determined, we obtain the rest of the conformal data as follows. The  
 118 solution of the bootstrap equations gives a spectrum of conformal dimensions  $\Delta_{\mathcal{O}}$  and structure  
 119 constants  $f_{\sigma\sigma\mathcal{O}}$  as a function of  $\Delta_\sigma$ ; they are divided into different sets characterized by the spin  
 120  $\ell = 0, 2, 4, \dots$  of the operator  $\mathcal{O}$ . The estimation of  $\Delta_{\mathcal{O}}$  and  $f_{\sigma\sigma\mathcal{O}}$  is obtained by taking the central  
 121 value of such quantities for  $\Delta_\sigma$  varying in the interval previously identified as the Ising point (grey  
 122 areas in Figs. 1 and 2). The error is obtained from their dispersion.

123 It is interesting to point out that, although we largely improved the precision of our results for  
 124  $4 > d > 3$  with respect to Ref. [20], we observe no signs of trouble associated to non-unitarity in  
 125 our bootstrap spectrum. On general grounds, non-unitarity contributions are expected to appear  
 126 for non-integer values of  $d$  due to the presence of negative-norm states [33]. However, these occur  
 127 at very high order in the OPE expansion of the correlator  $\langle \sigma\sigma\sigma\sigma \rangle$ , thus we may argue that they  
 128 have numerically negligible structure constants. As a matter of fact, their presence does not seem  
 129 to yield problems in solving the bootstrap equations with our method. This conclusion was also  
 130 reached by recent 3-correlator bootstrap studies of the critical  $O(N)$  models [18] and the Ising  
 131 model [21] in non-integer space dimensions using the navigator method [37].

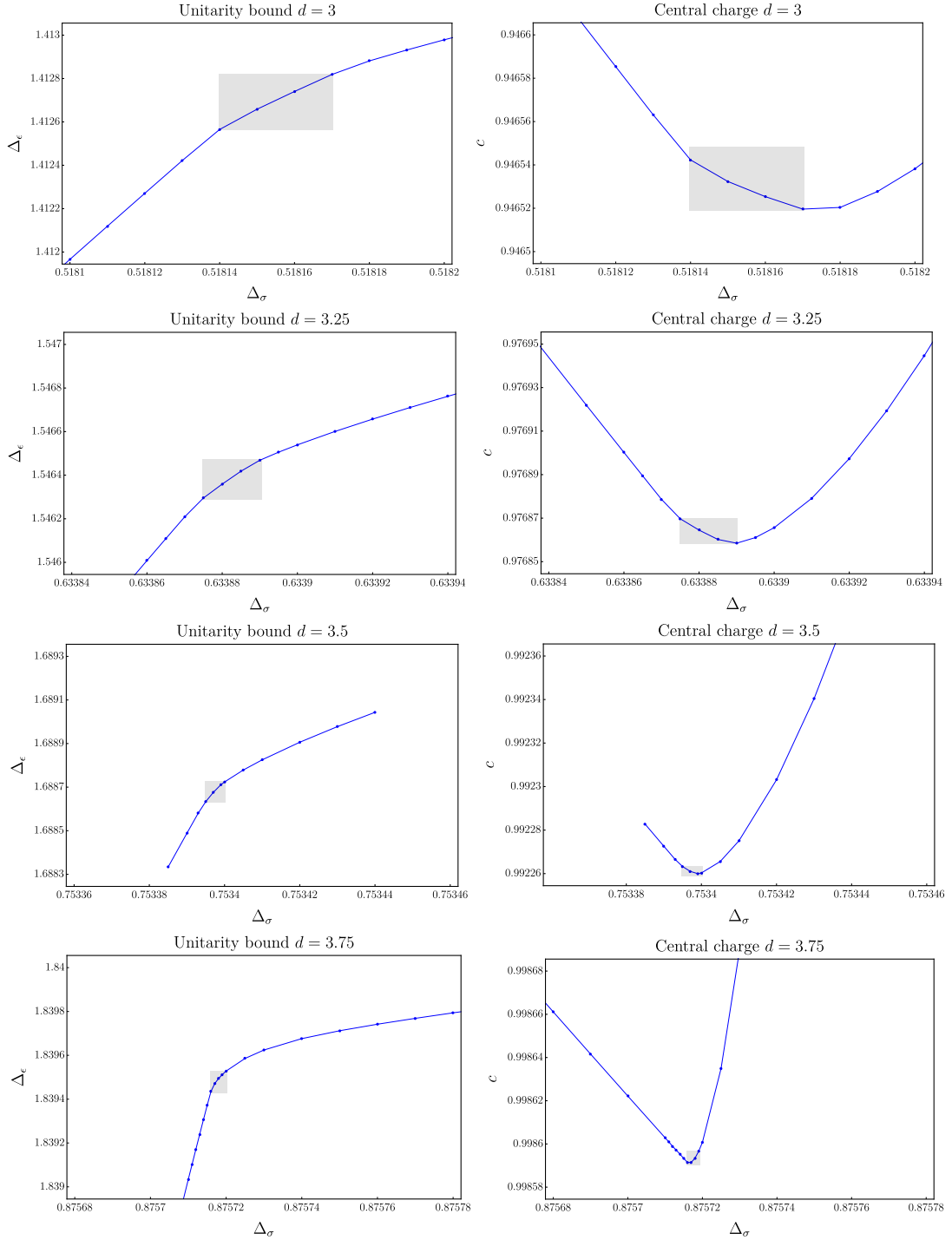


**Figure 1:** Determination of the Ising critical point for  $d = 3, 3.25, 3.5, 3.75$  ( $d = 3$  data from Ref. [20]). Left plots: Identification of the kink; the blue points correspond to the solutions of the bootstrap equations. Right plots: position of the  $c$  minimum. The grey shaded areas represent the estimated errors on  $\Delta_\sigma$ ,  $\Delta_\epsilon$  and  $c$ .

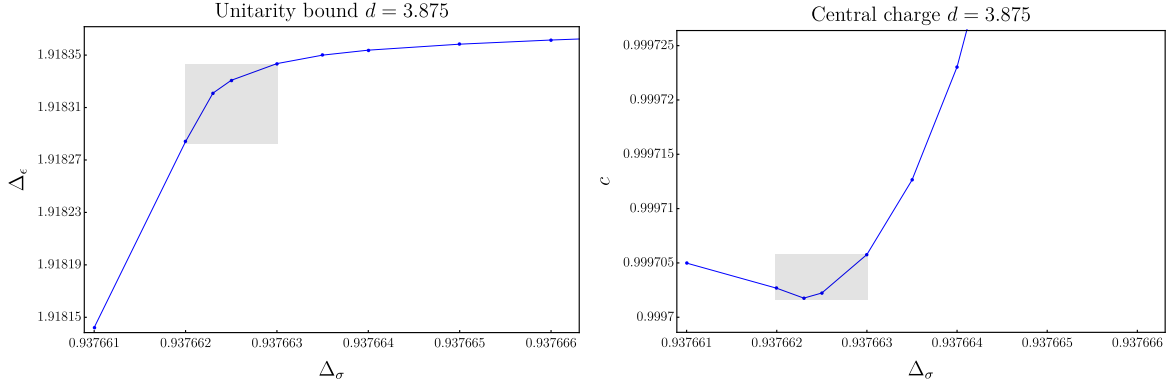


**Figure 2:** Determination of the Ising point for  $d = 3.875$ , as in Fig. 1. Note the magnified scale on both axis with respect to those of Fig. 1.

## 2.2 Analysis of conformal dimensions of the three leading fields for $4 > d \geq 3$

In Tab. 1 we present our results for the conformal dimensions  $\Delta_{\mathcal{O}}$  in  $4 > d > 3$  along with those of Ref. [20] for  $3 \geq d > 2$ , also employed in the following. Our implementation of the bootstrap determines with high precision the conformal dimensions and structure constants for the first few low-lying operators with  $\ell = 0, 2$  and 4:  $\mathcal{O}_{\ell=0} = \sigma, \epsilon, \epsilon'$ ,  $\mathcal{O}_{\ell=2} = T'$  and  $\mathcal{O}_{\ell=4} = C$  [20].

$d$	$\Delta_\sigma$	$\Delta_\epsilon$	$\Delta_{\epsilon'}$	$\Delta_{\epsilon''}$	$\Delta_{T'}$	$\Delta_C$	$\Delta_{C'}$
<b>4</b>	<b>1</b>	<b>2</b>	<b>4</b>	<b>6</b>	<b>6</b>	<b>6</b>	<b>8</b>
3.875	0.9376625(5)	1.91831(3)	3.992(2)	7.0(3)	5.9307(6)	5.8752253(9)	7.903(3)
3.75	0.8757175(15)	1.83948(4)	3.9771(12)	6.8(2)	5.8616(12)	5.75111(13)	7.81(3)
3.5	0.753398(3)	1.68868(5)	3.9296(8)	6.82(7)	5.734(7)	5.5053(5)	7.55(6)
3.25	0.633883(8)	1.54639(9)	3.8776(11)	6.92(6)	5.59(2)	5.264(2)	7.25(10)
3	0.518155(15)	1.41270(15)	3.8305(15)	7.01(5)	5.505(10)	5.026(4)	6.7(2)
2.75	0.40747(4)	1.2887(2)	3.800(2)	7.12(8)	5.445(15)	4.790(5)	6.3(2)
2.5	0.30341(1)	1.17625(15)	3.7970(10)	7.32(2)	5.46(3)	4.574(9)	5.78(13)
2.25	0.20822(3)	1.0784(2)	3.847(1)	7.53(2)	5.58(5)	4.344(14)	5.36(6)
2.2	0.19053(8)	1.0610(5)	3.864(4)	7.64(3)	5.69(4)	4.325(15)	5.29(4)
2.15	0.17333(8)	1.0444(4)	3.891(6)	7.73(3)	5.64(13)	4.28(3)	5.19(1)
2.1	0.15663(8)	1.0286(5)	3.9215(5)	7.82(3)	5.820(10)	4.17(4)	5.12(4)
2.05	0.14048(8)	1.0134(7)	3.9565(5)	7.93(3)	5.9050(10)	4.13(6)	5.065(15)
2.01	0.12803(8)	1.001(2)	3.9900(10)	8.035(5)	5.9815(5)	4.01440(10)	5.0115(15)
2.00001	0.125000(10)	0.99989(14)	4.0002(2)	7.99(10)	6.0006(2)	4.000055(10)	5.00048(8)
<b>2</b>	<b>0.125</b>	<b>1</b>	<b>4</b>	<b>8</b>	<b>6</b>	<b>4</b>	<b>5</b>

**Table 1:** Conformal dimensions of the first few low-lying states for  $4 > d > 2$ . Exact values for  $d = 2, 4$  are given in bold, results for  $3 \geq d > 2$  are taken from Ref. [20].

The goal of this section is to determine the behavior of  $\Delta_{\mathcal{O}}$  as a function of the variable  $y = 4 - d$ , by finding the best fitting polynomial that describes the data in Tab. 1. We use all available values, but focus on the range  $4 > d \geq 3$  where results are more precise and allow for a comparison with other approaches. The points for  $3 > d \geq 2$  are mainly used for stabilizing the higher powers of

141 the fitting polynomials<sup>3</sup>.

142 We employ an improved fit method for  $\Delta_{\mathcal{O}}(y)$  that uses orthogonal polynomials [49]: the idea is  
 143 to express the  $n^{\text{th}}$ -order polynomial fit function  $f_n(y)$  in terms of orthogonal polynomials  $P_k(y)$   
 144 of degree  $k = 0, 1, \dots, n$ , instead of a parameterization in terms of monomials,  $1, y, y^2, \dots, y^n$ . To  
 145 this aim we write

$$f_n(y) = \sum_{k=0}^n \alpha_k P_k(y), \quad \langle P_r(y) P_s(y) \rangle \propto \sum_{i=1}^{14} P_r(y_i) P_s(y_i) \propto \delta_{rs}, \quad (1)$$

146 where  $y_i$  are the values in Tab. 1. This method is equivalent to the naive one, but is numerically  
 147 more stable and the fit parameters  $\alpha_k$  can be determined with improved precision and less statistical  
 148 noise.

149 The optimal degree  $n$  for the fitting polynomial is not known *a priori* and is determined in the  
 150 following way: The fit with weights proportional to the inverse square of errors is done for several  
 151 values of  $n$ , and the least chi-square  $\chi_{\min}^2$  is found as a function of  $n$ . At a given order  $\bar{n}$ , adding  
 152 a further term  $\alpha_{\bar{n}+1} P_{\bar{n}+1}$  results in a negligible change of  $\chi_{\min}^2$  and the best fit yields a result for  
 153  $\alpha_{\bar{n}+1}$  which is compatible with zero within errors. This identifies  $\bar{n}$  as the degree of the optimal  
 154 polynomial. Finally, we use the results of our best fit for  $\{\alpha_k\}$  to assign an error to  $f_n(y)$  in the  
 155 whole range of  $4 > d \geq 3$ . Details on the fitting procedure and the computation of errors can be  
 156 found in App. A.

157 In this section we focus on the three leading operators  $\sigma, \epsilon$  and  $\epsilon'$  (corresponding to  $\phi, \phi^2$  and  
 158  $\phi^4$  in the  $\phi^4$  field theory), which are determined with very good precision. The analysis of higher-  
 159 dimensional operators is postponed to Sec. 4.2. Instead of working with conformal dimensions, we  
 160 consider the anomalous dimensions

$$\gamma_{\sigma} = \Delta_{\sigma} - \frac{d-2}{2}, \quad \gamma_{\epsilon} = \Delta_{\epsilon} - (d-2), \quad \gamma_{\epsilon'} = \Delta_{\epsilon'} - 2(d-2). \quad (2)$$

161 They are related to the Ising critical exponents  $\eta, \nu$  and  $\omega$  by

$$\eta = 2\gamma_{\sigma}, \quad \frac{1}{\nu} = 2 - \gamma_{\epsilon}, \quad \omega = d - 4 + \gamma_{\epsilon'}. \quad (3)$$

162 The vanishing of anomalous dimensions in the free theory ( $d = 4$ ) is assumed in the following fits.

163 Our analysis starts by comparing the old [20] and new data for  $4 > d > 3$ . In Fig. 3 the new  
 164 results (blue circles) show much smaller errors than the earlier findings (red crosses), due to a more  
 165 accurate localization of the Ising point, as explained above. In these and later figures we report the  
 166 differences ( $\gamma_{\mathcal{O}} - \text{fit}$ ) between data and fitting polynomial, because simpler plots would not capture  
 167 the small errors involved (note that the abscissas of the three plots differ by factors of ten). The  
 168 explicit form of the best fitting polynomials are provided in Sec. 3.

169 Next, we compare these results with those recently obtained by solving the 3-correlator bootstrap  
 170 with the navigator method [21]. In Fig. 4 our data, given in earlier figures (blue circles), are shown  
 171 on a finer scale, together with the estimated error of the fit (cyan shaded area). The red triangles  
 172 are the navigator values: they come with no errors and thus cannot be directly used for the fits<sup>4</sup>.

<sup>3</sup>Note that the lower quality of  $3 > d > 2$  data is due to the coarse scanning of  $\Delta_{\sigma}$  values, not to an intrinsic limitation of the numerical bootstrap approach [20].

<sup>4</sup>Earlier results of Ref. [19] are not considered here due to their large errors.

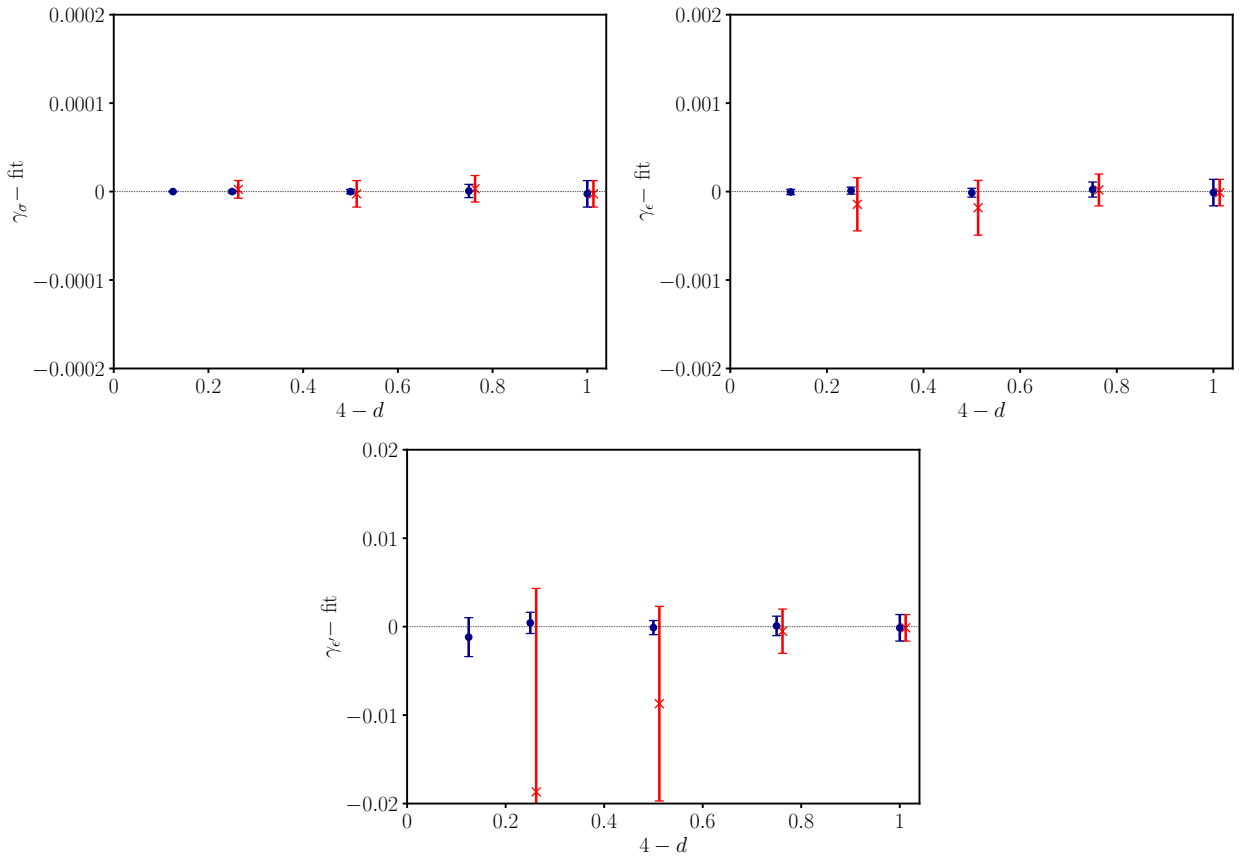


**Figure 3:** Old [20] (red crosses) and new (blue circles) bootstrap data for  $\gamma_\sigma, \gamma_\epsilon, \gamma_{\epsilon'}$ , minus the corresponding best fits. The plots use the same scales as in Ref. [20].

173 A first observation is the fairly good agreement between the two different bootstrap approaches at  
 174 our level of precision.

175 We propose to estimate the error of navigator data as follows. We suppose that they are roughly  
 176 of the same size as those found in other 3-correlator studies at  $d = 3$  (rigorous bounds) [48,50], which  
 177 are plotted in Fig. 4 as black diamonds ( $\gamma_\sigma$  and  $\gamma_\epsilon$ ), and a grey rightward triangle ( $\gamma_{\epsilon'}$ ). Assuming  
 178 these very small uncertainties for each value of  $d$ , there seems to be a negative offset with respect to  
 179 our data, in particular for  $\epsilon'$ . This could be a systematic error due to our approximate identification  
 180 of the Ising point within the unitarity region (Section 2.1), while the navigator method rigorously  
 181 determines it within a unitarity island [37]. However, other explanations are possible.

182 In conclusion, taking into account these considerations, we enlarge the error estimate of our fits  
 183 to the shaded gray bands in Figs. 4, which correspond to the following bounds:

$$\frac{\text{Err}(\gamma_\sigma)}{\gamma_\sigma} \approx \frac{\text{Err}(\gamma_\epsilon)}{\gamma_\epsilon} \lesssim 1 \times 10^{-3}, \quad \frac{\text{Err}(\Delta_{\epsilon'})}{\Delta_{\epsilon'}} \lesssim 0.5 \times 10^{-3}, \quad 3.875 \geq d \geq 3. \quad (4)$$

184 Given the small value of anomalous dimensions for  $d \rightarrow 4$ , these imply extremely low absolute  
 185 errors,  $\text{Err}(\gamma_\sigma) = O(10^{-6})$  and  $\text{Err}(\gamma_\epsilon) = O(10^{-5})$  in this range, as spelled out in the following  
 186 sections. This allows us to give a precise comparison to other methods, as a benchmark for the  
 187 Ising universality class in non-integer dimensions.



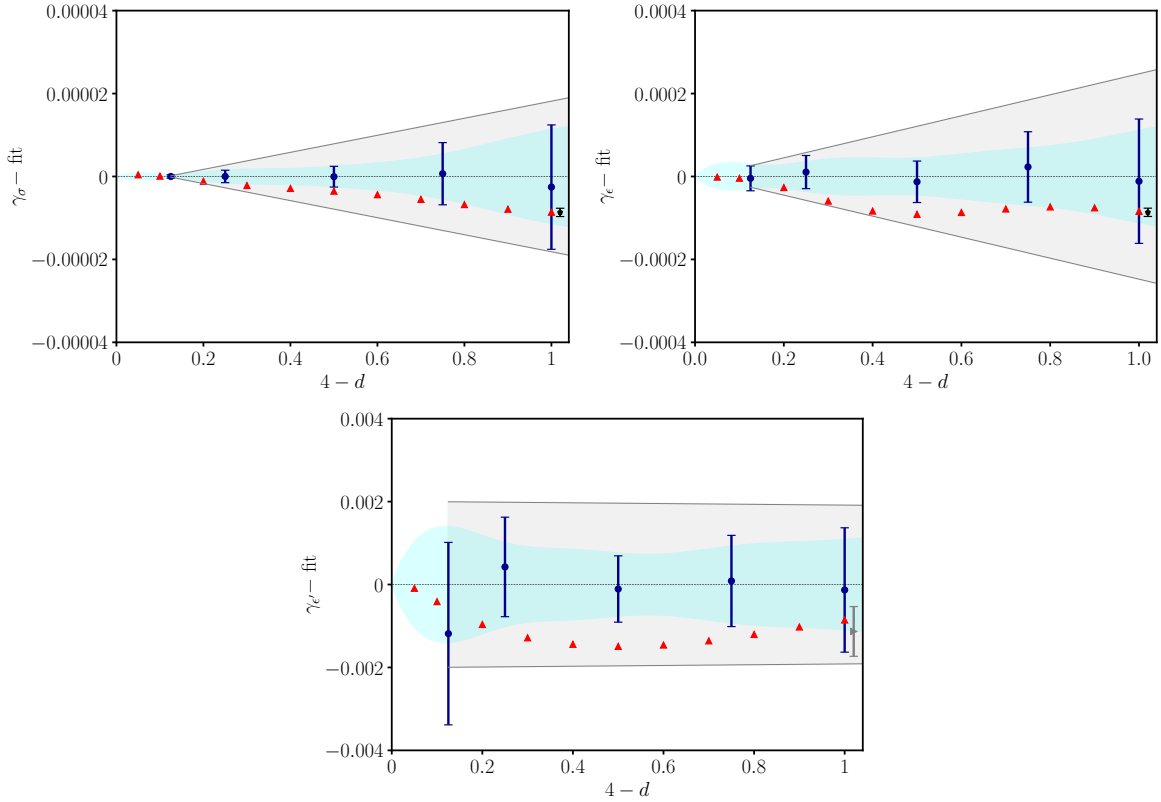


**Figure 4:** Plot of bootstrap data for  $\gamma_\sigma, \gamma_\epsilon, \gamma_{\epsilon'}$  minus the best fit values. The shaded area represents the error obtained from the  $\chi^2$  minimization of the fitting polynomial. The red triangles are results from Ref. [21] using the navigator method in a 3-correlator bootstrap setup (no error bars). Black diamonds and grey rightward triangle for  $d = 3$  represent respectively results by Ref. [48] ( $\gamma_\sigma$  and  $\gamma_\epsilon$ ) and Ref. [50] ( $\gamma_{\epsilon'}$ ); these data points are slightly displaced around  $d = 3$  to improve readability. The gray shaded bands represents the error bounds reported in Eq. (4).

### 188 3 Comparison with the epsilon expansion in $4 > d \geq 3$

189 In this section, we recall some features of the epsilon expansion and the resummation methods  
 190 employed for it. We compare unresummed and resummed series with the bootstrap results for  $\gamma_\sigma$ .  
 191 Then, the analysis is extended to  $\gamma_\epsilon$  and  $\gamma_{\epsilon'}$ .

#### 192 3.1 Warm-up analysis of the anomalous dimensions $\gamma_\sigma$

193 We start with a brief summary of the properties of the perturbative expansion of the  $\phi^4$  field  
 194 theory in  $d = 4 - y$ , which describes the Ising universality class. This is a textbook subject [51]  
 195 but we would like to single out a few aspects that are important in the following comparison with  
 196 bootstrap results in varying dimensions<sup>5</sup>.

197 The  $\beta$ -function  $\beta(g, y)$  and the anomalous dimensions  $\gamma_{\mathcal{O}}(g)$ , where  $\mathcal{O} = \phi, \phi^2, \phi^4$ , take the

<sup>5</sup>An up-to-date discussion of epsilon expansion can be found in Refs. [38–41]. We refer to these works for a proof of the following statements and appropriate referencing.

198 following form, in the Minimal Subtraction (MS) [51, 52] renormalization scheme,

$$\beta(g, y) = -yg + \sum_{k=2}^{n+1} \beta_k g^k, \quad \gamma_{\mathcal{O}}(g) = \sum_{k=1}^n \gamma_{\mathcal{O},k} g^k. \quad (5)$$

199 The numerical coefficients  $\beta_k, \gamma_{\mathcal{O},k}$  were computed up to order  $n = 6$  in Ref. [40], and  $n = 7$  in  
 200 Ref. [53]. While results up to order  $n = 15$  are known for a subclass of Feynman diagrams believed  
 201 to give the dominant contribution, they are not used here [40, 54].

202 The coefficients of the  $\beta$ -function (5) grow exponentially with  $k$ , and their asymptotic behavior  
 203 can be estimated from the contribution of instanton field configurations [51]

$$\beta_k \underset{k \rightarrow \infty}{\sim} C (-a)^k k^b k!. \quad (6)$$

204 Similar behaviors are found for the coefficients  $\gamma_{\mathcal{O},k}$ . The parameters  $a, b, C$  depend on the quantity  
 205 considered. One finds that the known values of the coefficients up to order  $n = 7$  grow very fast  
 206 with  $n$  but have not yet reached their asymptotic values (6) [40, 54].

207 The behavior (6) can be understood as follows: The perturbative series has a vanishing radius  
 208 of convergence in the complex  $g$  plane, because real negative values of  $g$  correspond to an upside-  
 209 down potential and an action not bounded from below. This fact can be exemplified by the simple  
 210 *zero-dimension path integral* (see App. B.1):

$$\mathcal{I}(g) = \int_{-\infty}^{\infty} \frac{dx}{\sqrt{2\pi}} e^{-\frac{x^2}{2} - gx^4} = \sum_{k=0}^{\infty} a_k (-g)^k, \quad a_k = \frac{(4k)!}{2^{2k}(2k)!k!} \underset{k \rightarrow \infty}{\sim} \frac{2^{4k}}{\sqrt{2\pi k}} \times k!. \quad (7)$$

211 This is the generating function counting the number of vacuum Feynman diagrams. The asymp-  
 212 totic behavior of  $a_k$  can be found by a saddle-point analysis of the integral. In field theory the  
 213 corresponding saddle point is given by instantons [51]<sup>6</sup>.

214 The solution of the fixed-point equation  $\beta(g, y) = 0$  gives  $g = g(y)$  by perturbative inversion  
 215 around  $g = y = 0$ ; this is used to rewrite the anomalous dimensions as a series in  $y$ ,

$$\gamma_{\mathcal{O}}(y) = \sum_{k=1}^n \bar{\gamma}_{\mathcal{O},k} y^k. \quad (8)$$

216 This is again a divergent series of asymptotic form (6), with suitable parameters  $a, b$  and  $C$ .

217 The ratio of two consecutive terms in the series (8) can be estimated from (6) as,  $\bar{\gamma}_{\mathcal{O},k} y / \bar{\gamma}_{\mathcal{O},k-1} \approx$   
 218  $-ak y$ , which is larger than one for  $y > 1/|ak|$ . A simple conclusion is that the more terms are  
 219 present in the perturbative series (8), the sooner it diverges as a series in  $y$ . We can draw two main  
 220 conclusions:

221 *i)* As it stands, the perturbative series (8) is basically useless for physical dimension  $y = 1$ , apart  
 222 from the first couple of terms, and resummation methods are necessary for extracting precise  
 223 values of anomalous dimensions. The resummation is based on the Borel transform, followed  
 224 by a conformal mapping, as will be explained later, and further discussed in App. B.1. This  
 225 procedure gives resummed finite expressions  $\tilde{\gamma}_{\mathcal{O}}(y)$ .

---

<sup>6</sup>There is growing consensus that the large-order behavior is governed by an instanton rather than a renor-  
 malon [54]. If one could go to much higher orders in the series expansion (e.g., 20-loop order) one could apply  
 methods of resurgence and trans-series [55].

226 *ii)* For dimensions close to  $d = 4$ , i.e.,  $y \ll 1$ , there is an optimal number of terms  $n_{\text{opt}}(y)$ , for  
 227 each  $y$  value, for which the distance between the series and the resummed function  $\tilde{\gamma}_{\mathcal{O}}(y)$ ,  
 228  $|\tilde{\gamma}_{\mathcal{O}}(y) - \sum_1^{n_{\text{opt}}} \bar{\gamma}_{\mathcal{O},k} y^k|$ , is minimal before growing again.

229 The perturbative anomalous dimensions  $\tilde{\gamma}_{\mathcal{O}}$  may differ from results obtained by other methods,  
 230 such as the lattice formulation of the path-integral for the Ising model, or by the bootstrap. These  
 231 differences are non-analytic, e.g.,  $\delta\gamma_{\mathcal{O}}(y) \sim \exp(-A/y)$ . Within the resummation procedure, these  
 232 terms may change according to how the inverse Borel transform is performed [55].

233 Before discussing the resummation methods in the next section, a first comparison of the per-  
 234 turbative expansion and the bootstrap data for  $\gamma_{\sigma}$  clarifies the issues at stake.

235 The perturbative series is [40, 53]

$$\begin{aligned} \gamma_{\sigma}(y) = & 0.00925926y^2 + 0.00934499y^3 - 0.00416439y^4 + 0.0128282y^5 \\ & - 0.0406363y^6 + 0.15738y^7, \quad (\text{epsilon expansion}). \end{aligned} \quad (9)$$

236 The best polynomial fit of bootstrap data in Tab. 1 using the methods outlined in Sec. 2.2 is<sup>7</sup>

$$\begin{aligned} \gamma_{\sigma}(y) = & 0.009306473y^2 + 0.008899908y^3 - 0.001435107y^4 + 0.001788710y^5 \\ & - 0.000533980y^6 + 0.000128667y^7, \quad (\text{conformal bootstrap}). \end{aligned} \quad (10)$$

237 The two polynomials (9) and (10) have different meanings, although their first two coefficients  
 238 are close. On one hand the Feynman-diagram series is exact, but has a vanishing radius of con-  
 239 vergence. On the other hand, the numerical bootstrap data in Tab. 1 should converge to exact  
 240 non-perturbative results upon increasing the numerical precision. The collection of these values  
 241 for any dimension  $d = 4 - y$  gives the exact function  $\gamma_{\sigma}^{\text{ex}}(y)$ , which however cannot be expressed  
 242 in terms of a simple polynomial. Therefore, the fit (10) gives approximated values around  $\gamma_{\sigma}^{\text{ex}}(y)$ ,  
 243 whose precision is *a priori* limited. Nonetheless, this description is sufficient at the present level of  
 244 numerical accuracy.

245 In Fig. 5 we show the difference between the perturbative series (9) and the bootstrap fit (10)  
 246 for  $4 > d \geq 3$ . Color lines correspond to the series (9) truncated at different orders  $n = 2, 3, \dots, 7$   
 247 (cf. color legend in the plot). One sees that, the higher the order  $n \geq 4$ , the sooner the perturbative  
 248 series diverges from the bootstrap data (corresponding to the zero horizontal line in Fig. 5). The  
 249 tiny errors of bootstrap points cannot be seen at this scale, thus showing that the unresummed  
 250 perturbative series cannot be used for a precise determination of critical exponents in  $d = 3$ , as  
 251 stated in point *ii)* above. Yet, the lower terms  $n = 2, 3$  may provide crude estimates.

252 Fig. 6 shows the other regime, close to four dimensions. Only the bootstrap point for  $d = 3.875$   
 253 is present in this range, but we also show results of Ref. [21] for  $d \geq 3.8$ , which match very well  
 254 while lacking error bars, as discussed earlier<sup>8</sup>. In contrast to the  $d \approx 3$  region, we observe that the  
 255 truncated perturbative series shows a different behavior. At any given  $y$  value, upon increasing the  
 256 perturbative order up to an optimal value  $n_{\text{opt}} \sim 1/y$ , the perturbative series approaches the zero  
 257 horizontal line (with a cyan error band), before starting to diverge. Namely, it matches the exact  
 258 bootstrap value  $\gamma_{\sigma}^{\text{ex}}(y)$ , within numerical errors.

<sup>7</sup>Note that the best-fit polynomial (10) starts with an  $O(y^2)$  term, because the linear term vanishes within errors. If a linear term is included in the fit procedure, it leads to a coefficient three orders of magnitude smaller than the quadratic term. Therefore, the conformal bootstrap implies  $\gamma_{\sigma}(y) = O(y^2)$  close to  $d = 4$ , in agreement with perturbation theory.

<sup>8</sup>Note that the red triangles are not used in our fit of bootstrap data.

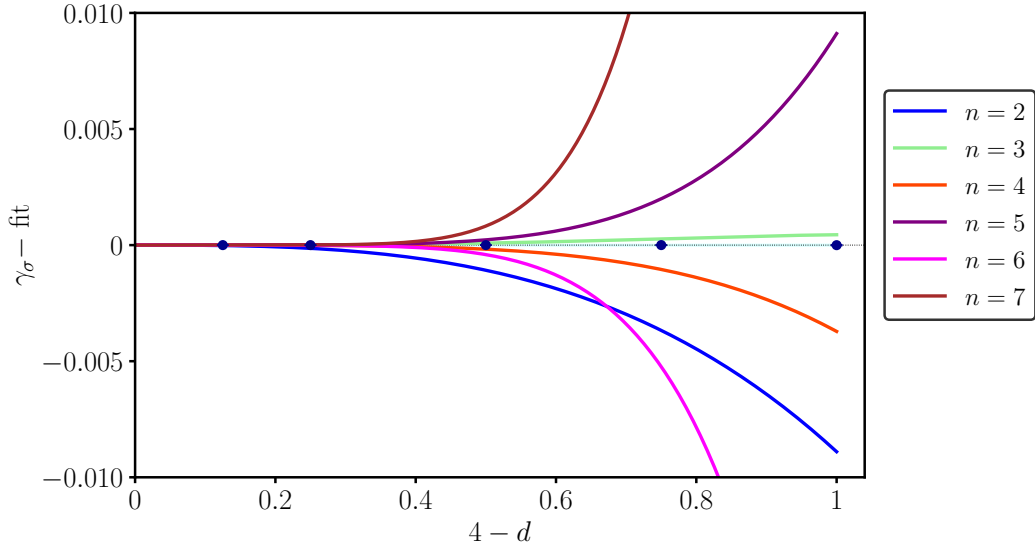


**Figure 5:** Comparison of  $\gamma_\sigma$  bootstrap data with unresummed epsilon expansion (9) in the region  $4 > d > 3$  for truncations of the series to order  $n = 2, \dots, 7$  (see color legend). All quantities have been subtracted by the best fit values (see (10)).

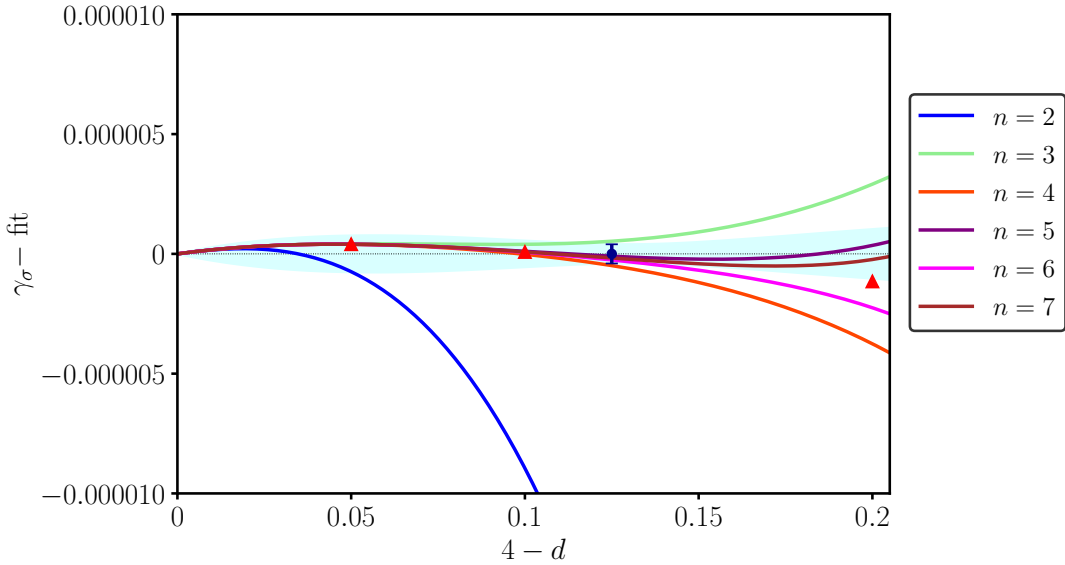


**Figure 6:** Comparison of  $\gamma_\sigma$  data minus best fit in the region  $4 > d > 3.8$ , between bootstrap (blue circle) and unresummed epsilon expansion (9) with different truncations of the perturbative series (cf. Fig. 5). The red triangles are the results of the bootstrap navigator method [21]. The cyan shaded area is the fit error.

259 Therefore, the comparison between non-perturbative bootstrap results and unresummed epsilon  
 260 expansion for  $\gamma_\sigma(y)$  is extremely good in the region  $4 > d > 3.8$ , with precision  $\text{Err}(\gamma_\sigma) \approx 1 \times 10^{-6}$ ,  
 261 i.e.,  $\text{Err}(\gamma_\sigma)/\gamma_\sigma < 1 \times 10^{-3}$ . According to the previous discussion, we conclude that we do not see  
 262 any non-perturbative difference for  $d \rightarrow 4$ .

263 We remark that the epsilon expansion can also be obtained by analytic solution of the bootstrap

264 equations around  $d = 4$ , assuming a perturbative expansion near the free theory [24,25,27,28,30–32].  
 265 Thus, is our comparison in Fig. 6 tautological? It is not, because the bootstrap identity is a set of  
 266 consistency conditions that depends on the kind of quantities they act on. Our numerical solution  
 267 does not assume any perturbative expansion, i.e., it is an independent solution of the bootstrap  
 268 constraints. That without any perturbative input, our conformal bootstrap results accurately  
 269 reproduce perturbative predictions close to  $d = 4$  is non-trivial.

270 A natural question is how our numerical bootstrap approach can reproduce the perturbative  
 271 series, i.e., in which regime the two polynomials (9) and (10) may agree beyond the  $O(y^3)$  term. As  
 272 said earlier, the bootstrap polynomial (10) is approximated, it can at most describe a band of values  
 273 around  $\gamma_\sigma^{\text{ex}}(y)$ . While the size  $\text{Err}(\gamma_\sigma)$  of this band stays finite in the whole range  $0 < y < 1$  (see  
 274 plots), that of the epsilon expansion is expanding in  $y$  and can be finite only for  $y < y_{\text{max}} \sim O(1/n)$ ,  
 275  $n$  being the perturbative order. We expect that, upon running the bootstrap for several points  $y_i$ ,  
 276 with  $0 < y_i < y_{\text{max}} \ll 1$ , and by performing best fits with polynomials limited to such a small  
 277 interval, one may find that the two expressions (9) and (10) match order by order, i.e., the epsilon  
 278 expansion is fully recovered.

### 279 3.2 Bootstrap data versus resummed perturbative results

280 Precise estimates of the critical exponents have been obtained over the years by refining the  
 281 resummation techniques applied to the epsilon expansion series [2–4,40,41,51,56,57]. In this work,  
 282 we use the methods of Refs. [40,41] extended to dimension  $4 > d \geq 3$ . Let us briefly recall the main  
 283 steps involved [51]. The Borel transform  $\mathcal{B}_{\gamma_\mathcal{O}}(t)$  of the perturbative expansion for the anomalous  
 284 dimension  $\gamma_\mathcal{O}$  (8) is defined by removing the factorial growth from the series,

$$\mathcal{B}_{\gamma_\mathcal{O}}(t) = \sum_{k=1}^n \frac{\tilde{\gamma}_{\mathcal{O},k}}{k!} t^k . \quad (11)$$

285 One infers from the asymptotic behavior (6) that this function has a singularity  $\mathcal{B}_{\gamma_\mathcal{O}}(t) \sim (1 +$   
 286  $ta)^{-b-1}$  and a corresponding finite radius of convergence.

287 The resummed quantity is defined by the inverse Borel transform,

$$\tilde{\gamma}_\mathcal{O}(y) = \int_0^\infty dt e^{-t} \mathcal{B}_{\gamma_\mathcal{O}}(yt). \quad (12)$$

288 By definition  $\gamma_\mathcal{O}(y)$  in (8) and  $\tilde{\gamma}_\mathcal{O}(y)$  in (12) have the same perturbative expansion; however, the  
 289 latter should be better behaved if  $\mathcal{B}_{\gamma_\mathcal{O}}(t)$  is suitably continued analytically outside the original disc  
 290  $|t| < 1/|a|$  to a region including the real positive axis<sup>9</sup>. Such analytic continuation in principle  
 291 requires the knowledge of all singularities of  $\mathcal{B}_{\gamma_\mathcal{O}}(t)$  in the complex  $t$ -plane. At this point, one can  
 292 only make educated guesses on these singularities, that translate into (physical) ansatzes for  $\tilde{\gamma}_\mathcal{O}(y)$ .

293 In practice, one assumes that the only singularity of  $\mathcal{B}_{\gamma_\mathcal{O}}(t)$  lies at  $t = -1/a$  real and negative,  
 294 and that it is a branch cut extending to  $t = -\infty$ . Using a conformal mapping  $t(z)$ , this branch cut  
 295 is mapped onto the unit circle, with the start of the branch cut mapped onto  $z = -1$ , and  $t = -\infty$   
 296 to  $z = 1$ , preserving the origin  $z = t = 0$ . As long as there are no other singularities,  $\mathcal{B}(t(z))$  has  
 297 a radius of convergence one in  $z$ . As  $t = \infty$  corresponds to  $z = 1$ , this allows one to perform the  
 298 inverse Borel transform (12). Details on this procedure can be found in App. B.1.

<sup>9</sup>In particular, a real negative value of the parameter  $a$  in (6), i.e., a perturbative series (8) of definite sign, is problematic.

299 This general idea can be improved in several ways, allowing one to introduce a set of free  
 300 parameters. The latter are determined such that the final result is the least sensible to their  
 301 variation. Apart from providing a robust resummation scheme, the parameter uncertainty implies  
 302 an estimate of the resummation error. These methods have been improved over the years by taking  
 303 into account the phenomenology of critical phenomena [51]. In our work, the resummed data are  
 304 obtained by extending the setup of Refs. [38, 40, 41] from  $d = 3$  to non-integer dimensions. A  
 305 complete account of these methods is too long to be presented here; nonetheless, we provide some  
 306 introductory material that will allow the reader to assess the original works. In App. B.1, the  
 307 resummation is worked out in a toy model, where one can compare it with the exact result. In  
 308 App. B.2, instead, a “reader’s guide” to Ref. [40] is presented, together with the values of the  
 309 resummation parameters used here.

310 Let us also mention that another option for the analytic continuation is to use Hypergeometric  
 311 functions, for which the inverse Borel transform can be written as a Meijer-G function [56]. One  
 312 drawback of this approach is the possibility for spurious poles on the integration contour. As here  
 313 we could not give justice to their influence, we exclude this resummation method.

314 Figure 7 shows the fitted bootstrap data (blue points) of  $\gamma_\sigma(y)$  already reported in Fig. 4, now  
 315 compared to the resummed epsilon-expansion values of Tab. 2 (green squares)<sup>10</sup>. The agreement  
 316 between these two results is very good, especially for  $d \geq 3.5$ , where the unresummed series (ma-  
 317 genta line) is already diverging, and greatly improves on earlier studies [2, 3] analyzed in [20]. Let  
 318 us remark that resummed  $\tilde{\gamma}_\sigma(y)$  values have been obtained for non-integer dimensions down to  
 319  $d = 2$ , still finding agreement with bootstrap data, although with larger uncertainties. Finally,  
 320 Fig. 7 shows the latest Monte Carlo results in  $d = 3$  (yellow rhombus), that match extremely well  
 321 the bootstrap points. Further  $d = 3$  results by these and other methods are summarized in a later  
 322 figure. Finally, Fig. 7 and later plots for the dimensions  $\gamma_\epsilon$  and  $\gamma_{\epsilon'}$  also report a solid red curve  
 323 linearly interpolating the navigator points of Ref. [21] obtained for  $4 > d \geq 3$ . This allows one to  
 324 assess the negligible difference between the two sets of bootstrap data in the comparison to the  
 325 epsilon-expansion.

$d$	$\Delta_\sigma$	$\Delta_\epsilon$	$\Delta'_\epsilon$
3.875	0.937662197(7)	1.91831086(14)	3.9924550(11)
3.75	0.8757158(3)	1.839419(4)	3.97529(3)
3.5	0.753393(10)	1.68854(7)	3.9276(5)
3.25	0.63386(8)	1.5458(4)	3.873(2)
3	0.5181(3)	1.4108(12)	3.820(7)

**Table 2:** Conformal dimensions of  $\sigma, \epsilon$  and  $\epsilon'$  field from resummed perturbative expansion, obtained according to the methods of [40].

<sup>10</sup>Resummations in this section use the 6-loop results, that were verified in several independent works [40, 41, 53]. We do not use the 7-loop results of Ref. [53], since they were not yet checked independently. Past experience, e.g., with the 5-loop results, teaches us that involved perturbative calculations require confirmation.

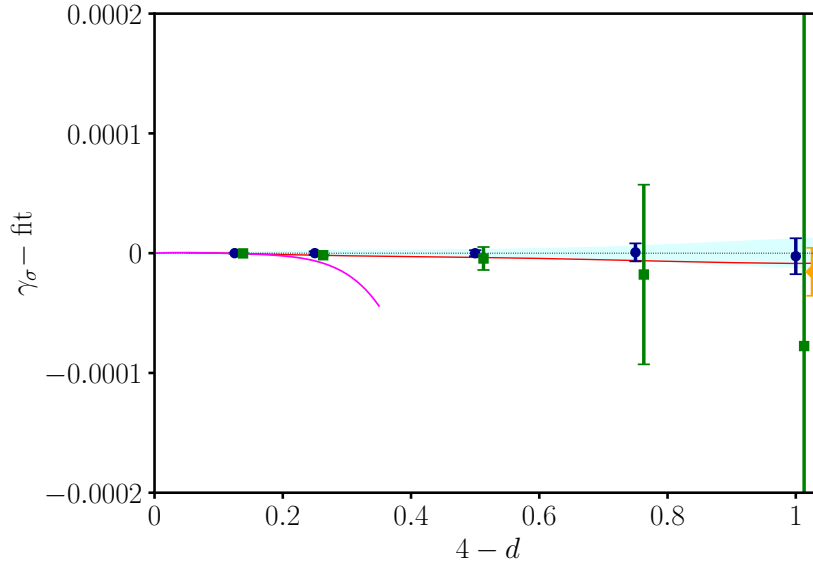


**Figure 7:** Comparison of  $\gamma_\sigma$  data minus best-fit values: bootstrap (blue circles), Borel-resummed epsilon expansion [40] (green squares), unresummed high-order epsilon expansion (magenta solid curve),  $d = 3$  Monte Carlo [44] (yellow rhombus). We also plot a solid red line linearly interpolating results of Ref. [21] for  $4 > d \geq 3$ . Note that data points are slightly displaced around the same  $d$  values ( $d = 3.875$ ,  $d = 3.75$ ,  $d = 3.5$ ,  $d = 3.25$  and  $d = 3$ ) to improve readability. Results from earlier work [3] have been omitted due to their large error bars.

326 We now extend the previous analysis to the energy field  $\epsilon$ . The best fit of the conformal bootstrap  
327 data is

$$\begin{aligned} \gamma_\epsilon(y) = & 0.333441601y + 0.114095325y^2 - 0.083458310y^3 \\ & + 0.081381007y^4 - 0.045296977y^5 + 0.014290102y^6 \\ & - 0.001741325y^7, \end{aligned} \quad (\text{conformal bootstrap}). \quad (13)$$

328 The epsilon-expansion series reads [40, 53]

$$\begin{aligned} \gamma_\epsilon(y) = & 0.3333333y + 0.117284y^2 - 0.124527y^3 + 0.30685y^4 - 0.95124y^5 \\ & + 3.57258y^6 - 15.2869y^7, \end{aligned} \quad (\text{epsilon expansion}). \quad (14)$$

329 One remarks the agreement, within errors, of the first two coefficients of this series; this corrects  
330 less precise results of [20] (cf. Fig. 6b there).

331 The comparison for  $d \rightarrow 4$  before resummation is shown in Fig. 8. As for Fig. 7, the truncated  
332 perturbative series for  $\gamma_\epsilon$  are plotted. Their curves approach the bootstrap fit (horizontal zero  
333 axis with cyan error band) with better and better precision. Note the remarkable quality of the  
334 navigator method (red triangles) [21]. Altogether, the agreement for  $d \rightarrow 4$  is found with high  
335 precision,  $\text{Err}(\gamma_\epsilon) = 3 \times 10^{-5}$  and  $\text{Err}(\gamma_\epsilon)/\gamma_\epsilon = 1 \times 10^{-3}$ .

336 Figure 9 presents a comparison with the resummed perturbative series (Tab. 2): the agreement  
337 is again very good for  $4 > d \geq 3.5$ ; there is a small  $O(10^{-3})$  deviation from the bootstrap and  
338 Monte Carlo results [44] (yellow rhombus) in  $d = 3$ . Probably there is a slight underestimation of  
339 the error. Let us remark that this resummation procedure is *honest*, as it does not use the exact

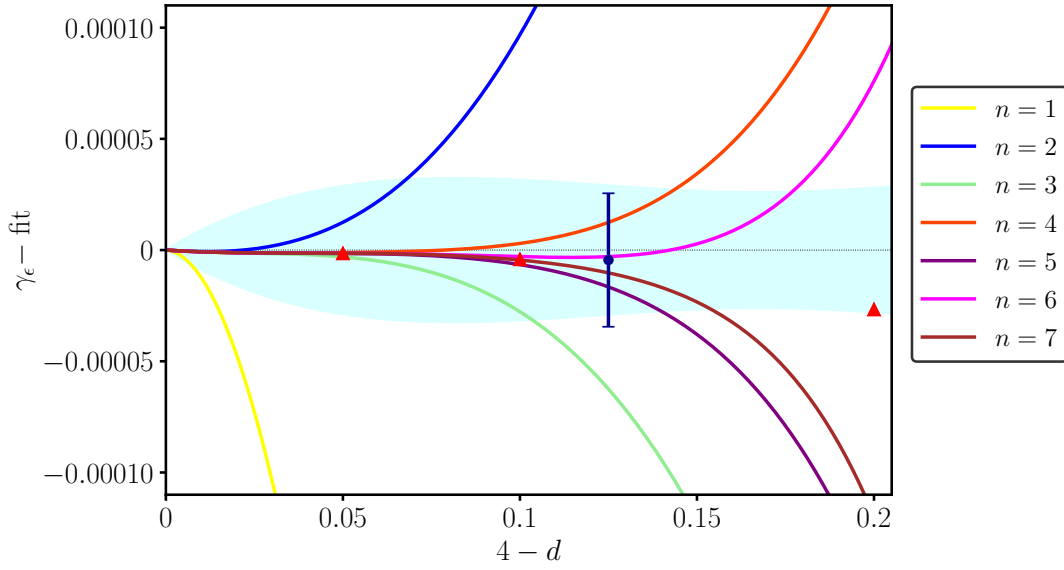


**Figure 8:** Comparison of the  $\gamma_\epsilon$  data minus the best fit in the region  $4 > d > 3.8$ . Our bootstrap point is the blue circle with error bar; the triangles are obtained by the navigator method [21]; the different truncations of the perturbative series are as in Fig. 5. The cyan shaded area is the fit error.

340  $d = 2$  conformal dimension as an input, with which it could be improved. The comparison with  
 341 another method, called Self-Consistent (SC) resummation<sup>11</sup> is presented in Fig. 10, where we plot  
 342 data of Tab. 3. In this case, the Borel transform is done on the perturbative series of  $1/\nu^3$ , instead  
 343 of  $1/\nu = 2 - \gamma_\epsilon$ : this choice is motivated by a match with the  $d = 2$  conformal field theory, that is  
 344 achieved through comparing the  $n$  dependence of the  $O(n)$ -symmetric  $\phi^4$  theory [41]. We conclude  
 345 that adding information of the exact results in  $d = 2$  improves the resummation of the perturbative  
 346 series (for this particular critical exponent). A similar constraint does not seem to be possible for  
 347 the other critical exponents, as discussed in Ref. [41].

$d$	$\Delta_\epsilon$
3.9	1.93440534057(12)
3.8	1.8706742(6)
3.7	1.808546(5)
3.6	1.747876(2)
3.5	1.68858(6)
3.4	1.63062(15)
3.3	1.5740(3)
3.2	1.5187(5)
3.1	1.4647(9)
3	1.4122(15)

**Table 3:** Conformal dimension of  $\epsilon$  field from resummed perturbative expansion, obtained according to the methods of [41].

<sup>11</sup>See Ref. [41] for a detailed discussion of this approach.



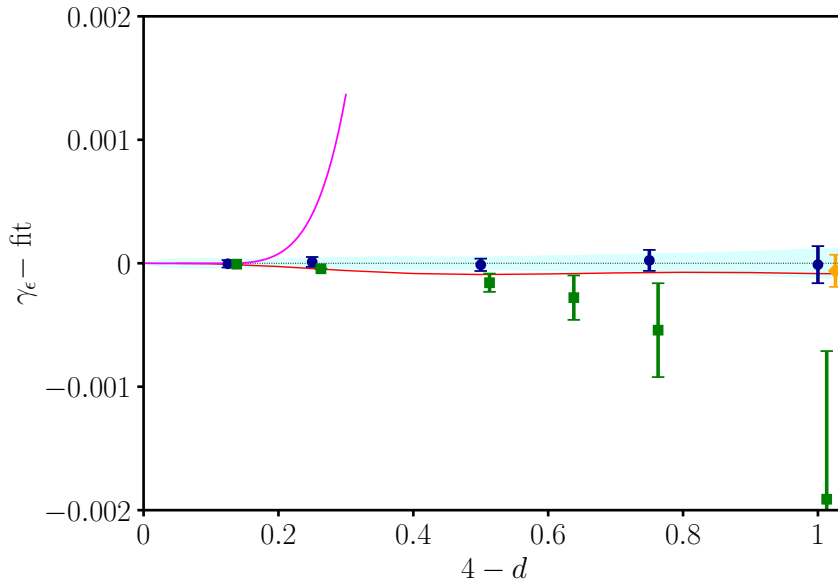


**Figure 9:** Comparison of  $\gamma_\epsilon$  data minus best fit: bootstrap (blue circles), Borel-resummed epsilon expansion [40] (green squares), unresummed epsilon expansion (magenta solid curve),  $d = 3$  Monte Carlo [44] (yellow rhombus). We also plot a solid red line linearly interpolating results of Ref. [21] for  $4 > d \geq 3$ . The cyan shaded area is the fit error as in earlier plots.

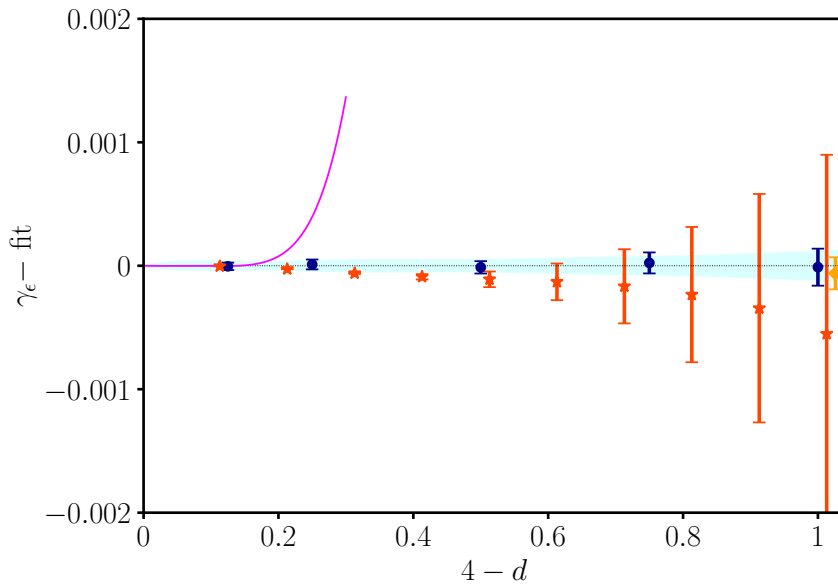


**Figure 10:** Comparison of  $\gamma_\epsilon$  minus best fit: bootstrap (blue circles), Self-Consistent resummed epsilon expansion [41] (red stars), unresummed epsilon expansion (magenta solid curve),  $d = 3$  Monte Carlo [44] (yellow rhombus).

348 Summarizing, the bootstrap and epsilon-expansion results agree very well: for  $d \rightarrow 4$  the unre-  
 349 summed series fits perfectly, for  $4 > d \geq 3$  there is remarkable agreement, keeping in mind that  
 350 the resummation error is roughly one order of magnitude larger than that of bootstrap and Monte

351 Carlo results.

352 A comparison of all  $d = 3$  results available in the literature for  $\gamma_\sigma$  and  $\gamma_\epsilon$  is given in Figs. 11  
 353 and 12. The corresponding numerical values are in Tab. 4. Besides data already discussed (drawn  
 354 in earlier colors), we report recent results of the non-perturbative renormalization group [45] (brown  
 355 downward triangle). The central value is given by our fit of the bootstrap data with error given by  
 356 the cyan band, not by the mean value of all results. The Figs. 11 and 12 respect our convention  
 357 of plotting the two anomalous dimensions on scales differing by one order of magnitude, roughly  
 358 equal to the ratio of their actual value. Finally, Tab. 4 and Figs. 11, 12 report also the results  
 359 of other 3-correlator bootstrap approaches, using EFM [48] and the navigator method [50], and  
 360 paying particular attention to error estimates (cf. rigorous bounds). We also remark that the  
 361 results obtained by perturbative expansions directly in  $d = 3$  [3, 4] are consistent with bootstrap  
 362 results too, but have one order of magnitude larger errors and are therefore not plotted in Figs. 11  
 363 and 12.

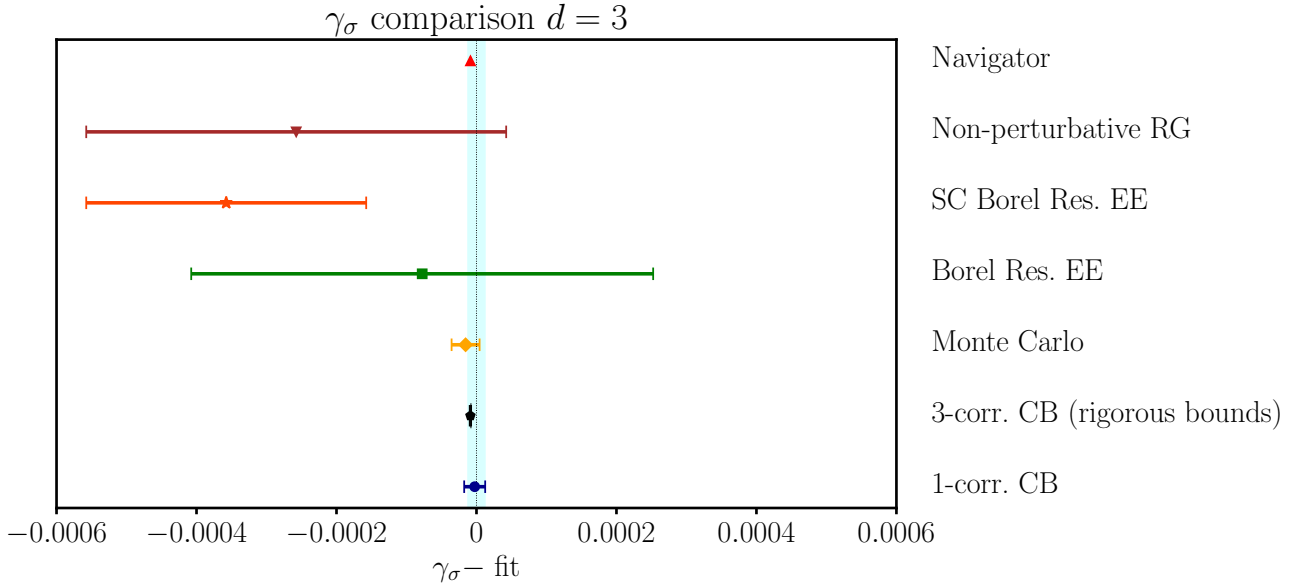


**Figure 11:** Summary of up-to-date predictions for  $\gamma_\sigma$  at  $d = 3$  (minus best fit): 1-correlator bootstrap [20] (blue circle), 3-correlator bootstrap with rigorous bounds [48] (black pentagon), Monte Carlo [44] (yellow rhombus), Borel-resummed epsilon expansion [40] (green square), Self-Consistent resummed epsilon expansion [41] (red star), non-perturbative renormalization group [45] (brown downward triangle), bootstrap navigator method [21] (red upward triangle).

364 We now analyze the subleading  $\mathbb{Z}_2$ -even scalar field  $\epsilon'$ , which is related to the critical exponent  
 365  $\omega = \Delta_{\epsilon'} - d = d - 4 + \gamma_{\epsilon'}$ . The best fit of our data gives<sup>12</sup>:

$$\begin{aligned}
 \gamma_{\epsilon'}(y) = & 2.000178549y - 0.518006835y^2 + 0.721996645y^3 \\
 & - 0.684437170y^4 + 0.447648598y^5 - 0.162903635y^6 \\
 & + 0.026155257y^7, \quad (\text{conformal bootstrap}). \quad (15)
 \end{aligned}$$

366 The large errors of the earlier analysis [20] have been reduced, as explained earlier (see Fig. 3). The

<sup>12</sup>The fit again assumes  $\gamma_{\epsilon'} = 0$  for  $d = 4$ .

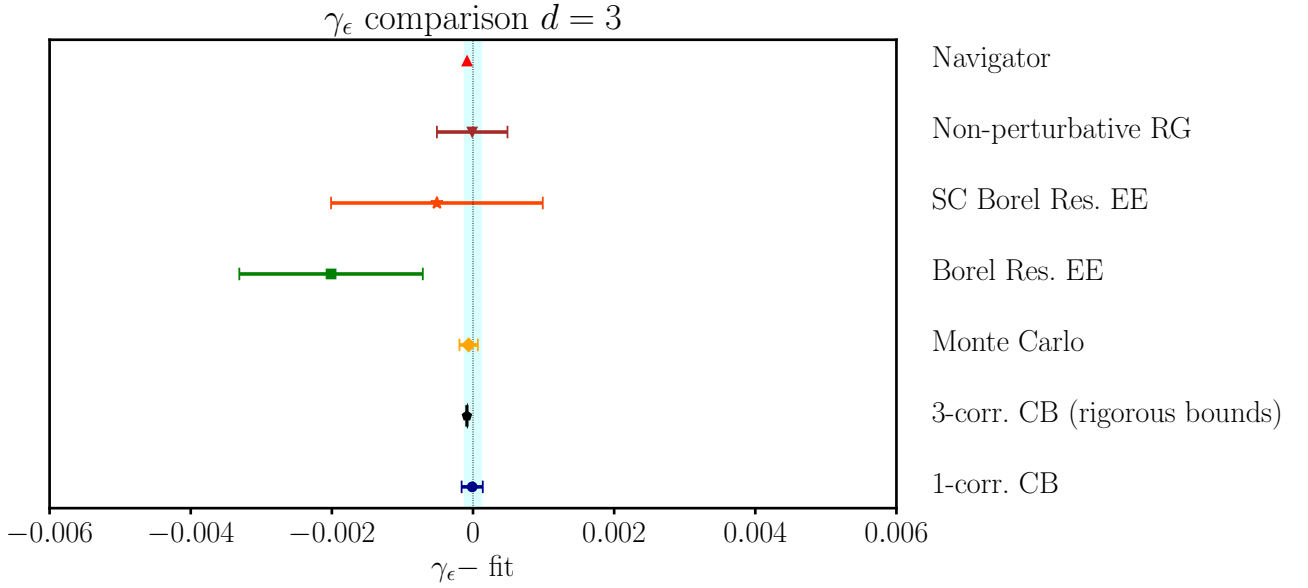


**Figure 12:** Summary of up-to-date predictions for  $\gamma_\epsilon$  in  $d = 3$  (minus best fit): 1-correlator bootstrap [20] (blue circle), 3-correlator bootstrap with rigorous bounds [48] (black pentagon), Monte Carlo [44] (yellow rhombus), Borel-resummed epsilon expansion [40] (green square), Self-Consistent resummed epsilon expansion [41] (red star), non-perturbative renormalization group [45] (brown downward triangle), bootstrap navigator method [21] (red upward triangle).

$d = 3$ Ising critical indices	$\Delta_\sigma$	$\Delta_\epsilon$	$\Delta_{\epsilon'}$
Bootstrap (1 correlator)	0.518155(15)	1.41270(15)	3.8305(15)
Bootstrap (3 correlators)	0.5181489(10)	1.412625(10)	3.8297(2)
Borel resummed epsilon expansion	0.5181(3)	1.4107(13)	3.820(7)
SC Borel resummed epsilon expansion	0.5178(2)	1.4122(15)	3.827(13)
Monte Carlo	0.51814(2)	1.41265(13)	3.832(6)
Non-perturbative RG	0.5179(3)	1.41270(50)	3.832(14)
Navigator (rigorous bounds)	0.518157(35)	1.41265(36)	3.8295(6)

**Table 4:** Comparison of  $d = 3$  results for the conformal dimensions of low-lying fields: 1-correlator bootstrap [20], 3-correlator bootstrap [48] (errors on  $\Delta_\sigma$  and  $\Delta_\epsilon$  are rigorous bounds), Borel-resummed epsilon expansion [40], Self-Consistent (SC) Borel-resummed epsilon expansion [41], Monte Carlo [42, 44], non-perturbative renormalization group [45, 46] and bootstrap navigator method with rigorous bounds [50].

367 epsilon-expansion series is [40, 53],

$$\begin{aligned} \gamma_{\epsilon'}(y) = & 2y - 0.62963y^2 + 1.61822y^3 - 5.23514y^4 + 20.7498y^5 \\ & - 93.1113y^6 + 458.7424y^7, \end{aligned} \quad (\text{epsilon expansion}). \quad (16)$$

368 In Fig. 13 we show the difference between the data and the bootstrap best fit (15). The overall  
369 error of the fit for  $\gamma_{\epsilon'}$  is estimated to be less than  $2.0 \times 10^{-3}$  in the whole range. The relative error

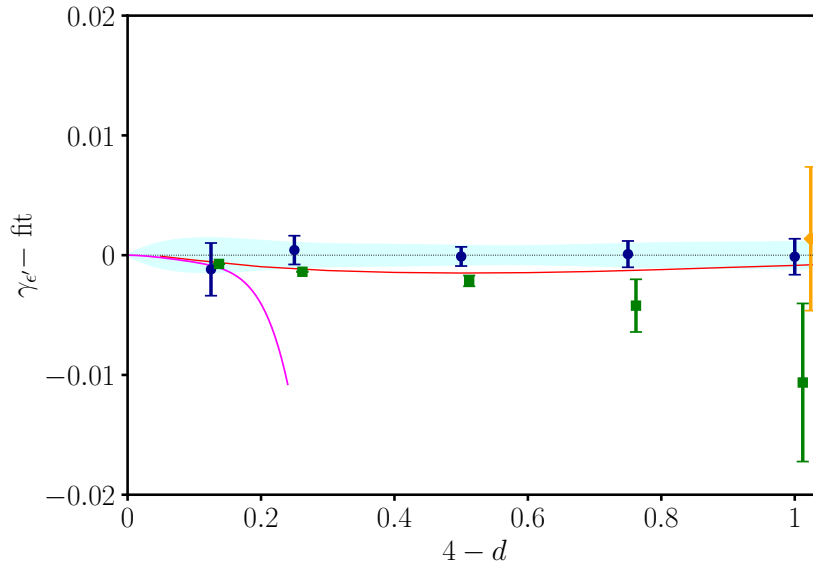


**Figure 13:** Comparison of  $\gamma_{\epsilon'}$  data minus best fit: bootstrap (blue circles), Borel-resummed epsilon expansion [40] (green squares), unresummed epsilon expansion (magenta solid curve),  $d = 3$  Monte Carlo [42] (yellow rhombus). We also plot a solid red line linearly interpolating results of Ref. [21] for  $4 > d \geq 3$ .

370 is  $\text{Err}(\gamma_{\epsilon'})/\gamma_{\epsilon'} = 1 \times 10^{-3}$  for  $d = 3$  but goes up to<sup>13</sup>  $1 \times 10^{-2}$  for  $d = 3.875$ . The comparison with  
 371 Monte Carlo [42, 44] in  $d = 3$ , and the resummed epsilon-expansion series are also shown, finding  
 372 again good agreement at the coarser scale (note a factor of 10 w.r.t. Fig. 9). A systematic difference  
 373 between bootstrap and epsilon-expansion points is seen for  $d \rightarrow 3$ , similar to what was found for  
 374  $\gamma_{\epsilon}$  in Fig. 9. Such a drift is smaller for the navigator results [21] (red line) than for our data, for  
 375  $4 > d \geq 3.5$ . Further values of  $\Delta_{\epsilon'}$  in  $d = 3$  found in the literature are reported in Tab. 4 and  
 376 plotted in Fig. 14. A zoom over the region close to  $d = 4$  is drawn in Fig. 15, showing the same  
 377 features as in Figs. 6 and 8.

378 We conclude this section by stressing the very good overall agreement of bootstrap and resummed  
 379 epsilon expansion. The study in varying dimensions clarifies the different behavior of quantities in  
 380 the perturbative and non-perturbative regimes.

<sup>13</sup>The growth of the error when passing from  $d = 3.75$  to  $d = 3.875$  is due to the instability of the higher part of the spectrum when approaching  $d = 4$ . This issue is further discussed in Sec. 4.3.

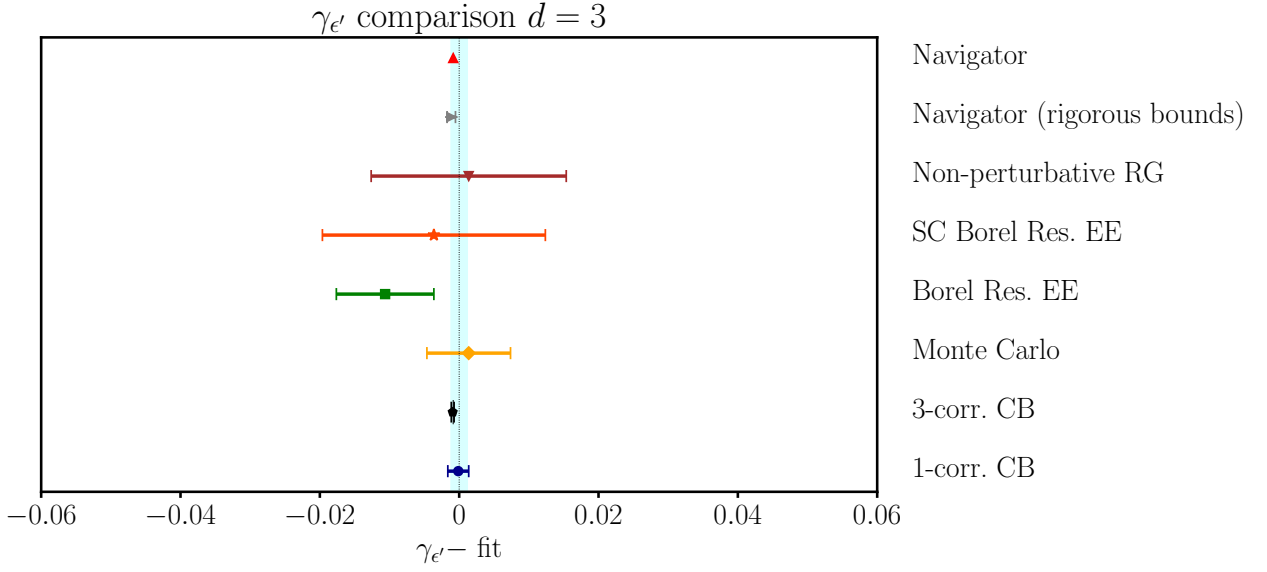


**Figure 14:** Summary of up-to-date predictions for  $\gamma_{\epsilon'}$  in  $d = 3$  (minus our best fit, from bottom to top): 1-correlator bootstrap [20] (blue circle), 3-correlator bootstrap [48] (black pentagon), Monte Carlo [44] (yellow rhombus), Borel-resummed epsilon expansion [40] (green square), Self-Consistent resummed epsilon expansion [41] (red star), non-perturbative renormalization group [45] (brown downward triangle), bootstrap navigator method with rigorous bounds [50] (grey rightward triangle), bootstrap navigator method [21] (red upward triangles).

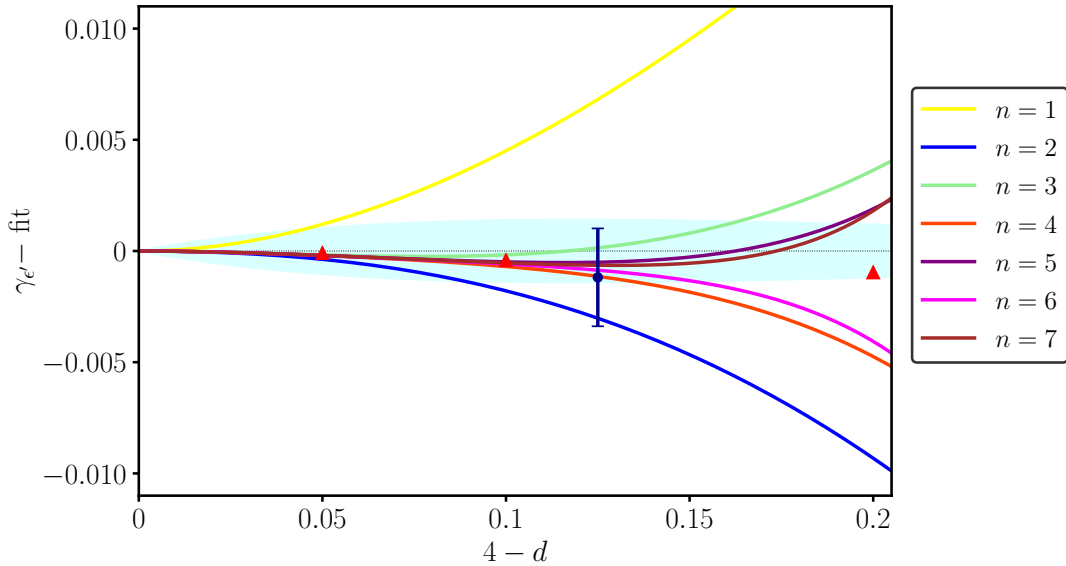


**Figure 15:** Comparison of the  $\gamma_{\epsilon'}$  data minus the best fit in the region  $4 > d > 3.8$ . Our bootstrap point is the blue circle with error bar; the triangles are obtained by the navigator method [21]; the different truncations of the perturbative series are as in Fig. 5. The cyan shaded area is the fit error.

## 4 Structure constants and scaling dimensions of higher fields

In this section we analyze further bootstrap data. The structure constants (OPE coefficients) of low-lying fields  $\sigma, \epsilon, \epsilon', T$  are very precise, the error being on the fifth decimal, thus better than those of the corresponding conformal dimensions presented earlier. Next we discuss subleading and spinful fields,  $\epsilon'', T', C, C'$ , presenting results for both dimensions and structure constants. Some of them are good, others are not completely correct, showing the limits of our numerical bootstrap approach.

### 4.1 Structure constants in $4 > d \geq 3$

Tab. 5 reports all data for structure constants: those for  $4 > d > 3$  are new results, the ones for  $3 \geq d > 2$  are taken from [20]. The central charge  $c$  is obtained from the structure constant  $f_{\sigma\sigma T}$  of the energy-momentum tensor  $T$  by

$$f_{\sigma\sigma T}^2 = \frac{d}{4(d-1)} \frac{\Delta_\sigma^2}{c}. \quad (17)$$

For  $f_{\sigma\sigma\mathcal{O}}$ , we adopt the by-now standard normalization of [21, 48]. The relation with the earlier normalization  $\tilde{f}_{\sigma\sigma\mathcal{O}}$  of Ref. [15] is

$$f_{\sigma\sigma\mathcal{O}}^2 = \frac{\left(\frac{d-2}{2}\right)_\ell}{(d-2)_\ell} \tilde{f}_{\sigma\sigma\mathcal{O}}^2, \quad (18)$$

where  $(x)_\ell \equiv \Gamma(x+\ell)/\Gamma(x)$  is the Pochhammer symbol.

The central charge  $c$  and the structure constants  $f_{\sigma\sigma\epsilon}$  and  $f_{\sigma\sigma\epsilon'}$  are determined with very high accuracy: their dependence on  $y = 4 - d$  is obtained with the fit method of Sec. 3.1, assuming

$d$	$c$	$f_{\sigma\sigma\epsilon}$	$f_{\sigma\sigma\epsilon'}$	$f_{\sigma\sigma\epsilon''} \times 10^4$	$f_{\sigma\sigma T'}$	$f_{\sigma\sigma C}$	$f_{\sigma\sigma C'}$
<b>4</b>	<b>1</b>	<b>1.4142136</b>	<b>0</b>	<b>0</b>	<b>0</b>	<b>0.169031</b>	<b>0</b>
3.875	0.99970(2)	1.38228(2)	0.015298(14)	0.33(10)	0.003070(2)	0.1540603(3)	0.000772(2)
3.75	0.998594(3)	1.34586(3)	0.027517(15)	1.4(3)	0.005641(5)	0.133(8)	0.00134(10)
3.5	0.9922615(15)	1.26132(3)	0.04426(3)	4.0(2)	0.00911(10)	0.105(5)	0.0021(3)
3.25	0.976864(6)	1.16282(4)	0.05225(3)	6.0(3)	0.0106(2)	0.084(6)	0.0019(9)
3	0.946535(15)	1.05184(4)	0.05300(5)	7.1(4)	0.010575(15)	0.065(5)	0.0020(5)
2.75	0.893275(15)	0.92939(4)	0.04794(8)	7.0(4)	0.00901(6)	0.048(4)	0.00235(15)
2.5	0.807110(10)	0.796303(5)	0.03885(2)	5.90(9)	0.00668(3)	0.033(3)	0.0029(3)
2.25	0.677724(2)	0.65311(2)	0.02738(4)	4.27(5)	0.00394(14)	0.0195(15)	0.0035(2)
2.2	0.64609(7)	0.62333(6)	0.0245(5)	3.76(9)	0.00352(7)	0.019(4)	0.0038(3)
2.15	0.61243(8)	0.59313(8)	0.0225(5)	3.36(2)	0.0025(5)	0.017(3)	0.00385(15)
2.1	0.57680(10)	0.56249(7)	0.02018(8)	2.98(7)	0.00265(5)	0.016(3)	0.00395(15)
2.05	0.53935(15)	0.53143(8)	0.01785(5)	2.58(4)	0.00230(10)	0.0135(25)	0.00390(10)
2.01	0.5082(3)	0.5058(6)	0.01605(5)	2.246(9)	0.00193(3)	0.01550(10)	0.003920(10)
2.00001	0.500015(15)	0.499998(5)	0.015623(4)	2.0(2)	0.0018520(5)	0.0148235(15)	0.0039040(10)
<b>2</b>	<b>0.5</b>	<b>0.5</b>	<b>0.0156250</b>	<b>2.1972656</b>	<b>0.00185290</b>	<b>0.0148232</b>	<b>0.003906</b>

**Table 5:** Structure constants of the first few low-lying states for  $4 > d > 2$ . The exact values for  $d = 2, 4$  are given in bold, results for  $3 \geq d > 2$  are taken from [20].

397 the exact  $d = 4$  value. The resulting polynomials are reported together with the available epsilon-  
 398 expansion series [30, 31, 58, 59]:

$$c(y) = 1 - 0.015415049y^2 - 0.026663929y^3 - 0.004992140y^4 - 0.010357094y^5 + 0.007424814y^6 - 0.004670278y^7 + 0.001206599y^8, \quad (\text{conformal bootstrap}), \quad (19)$$

$$c(y) = 1 - 0.0154321y^2 - 0.0266347y^3 - 0.0039608y^4, \quad (\text{epsilon expansion}), \quad (20)$$

399

$$f_{\sigma\sigma\epsilon}(y) = \sqrt{2} - 0.235465537y - 0.170275458y^2 + 0.096635030y^3 - 0.113371408y^4 + 0.100586943y^5 - 0.054667196y^6 + 0.016161292y^7 - 0.001992399y^8, \quad (\text{conformal bootstrap}), \quad (21)$$

$$f_{\sigma\sigma\epsilon}(y) = \sqrt{2} - 0.235702y - 0.168047y^2 + 0.103680y^3 - 0.224776y^4, \quad (\text{epsilon expansion}), \quad (22)$$

400

$$f_{\sigma\sigma\epsilon'}(y) = 0.136221303y - 0.118250195y^2 + 0.067116467y^3 - 0.058700794y^4 + 0.037159615y^5 - 0.012211017y^6 + 0.001647332y^7, \quad (\text{conformal bootstrap}), \quad (23)$$

$$f_{\sigma\sigma\epsilon'}(y) = 0.1360828y + 0.11844240525y^2, \quad (\text{epsilon expansion}). \quad (24)$$

401 We remark: *i*) the excellent agreement between the first few terms of the conformal bootstrap and  
 402 epsilon-expansion series, and *ii*) the need of a high-order  $O(y^7, y^8)$  polynomial for precise fits. The  
 403 corresponding curves are shown in Figs. 16 and 17. Note that  $c$ ,  $f_{\sigma\sigma\epsilon}$  and  $f_{\sigma\sigma\epsilon'}$  were determined  
 404 with strikingly small (relative) errors, respectively  $O(10^{-5})$ ,  $O(10^{-4})$  and  $O(10^{-4})$  over the entire  
 405  $d$  range.

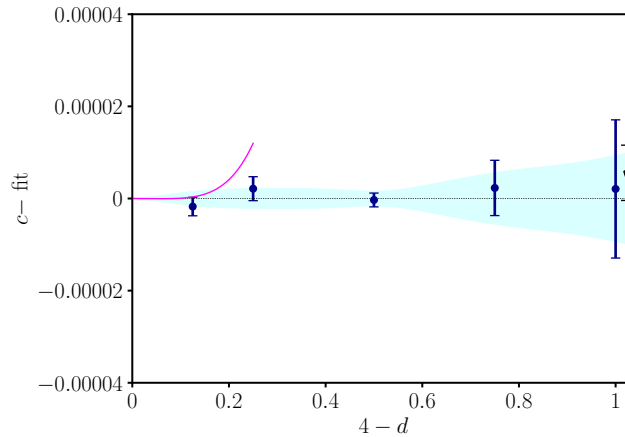


**Figure 16:** Comparison of  $c$  data minus best fit: bootstrap (blue circles), unresummed epsilon expansion [58, 59] (magenta solid curve), 3-correlator bootstrap at  $d = 3$  [48] (black pentagon).

406 The comparison with other conformal bootstrap results is as follows: The best 3-correlator  
 407 determination in  $d = 3$  [48] is shown as a black pentagon in the figures. Data from the navigator

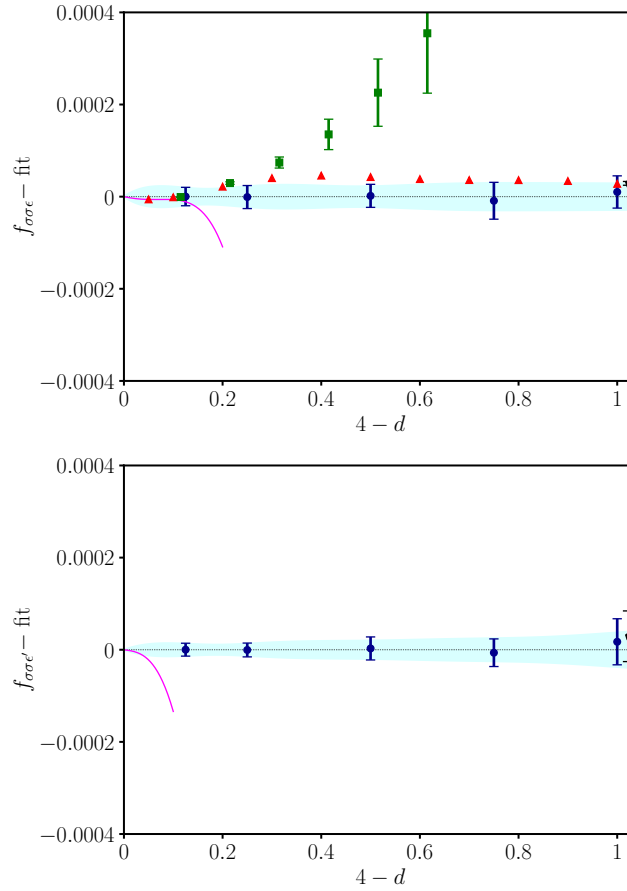


**Figure 17:** Comparison of  $f_{\sigma\sigma\epsilon}$  and  $f_{\sigma\sigma\epsilon'}$  minus best fit: bootstrap (blue circles), unresummed epsilon expansion [30, 31, 58, 59] (magenta solid curve), 3-correlator bootstrap at  $d = 3$  [48] (black pentagon). For  $f_{\sigma\sigma\epsilon}$  we also report the resummed epsilon expansion (green squares) and bootstrap navigator results [21] (red triangles).

408 method are unfortunately only available for  $f_{\sigma\sigma\epsilon}$  [21]. The agreement among different numerical  
 409 setups is extremely good. Moreover, as already observed for scaling dimensions, the unresummed  
 410 epsilon expansion captures the  $d \rightarrow 4$  behavior, and it does it very well, since the lower-order  
 411 terms of the respective polynomials (19)–(24) are equal within errors. For  $f_{\sigma\sigma\epsilon}$ , the results of the  
 412 resummed epsilon expansion, reported in Tab. 6, are also shown, determined by earlier methods:  
 413 the 4<sup>th</sup>-order series (22) only allows for a precise agreement down to  $d \approx 3.6$ , given the fine scale of  
 414 Fig. 17. For the remaining quantities, the epsilon expansion is either too short for a resummation,  
 415 or not alternating.



$d$	$f_{\sigma\sigma\epsilon}$
3.9	1.3890497(2)
3.8	1.360960(3)
3.7	1.330222(12)
3.6	1.29703(3)
3.5	1.26154(7)
3.4	1.22386(13)
3.3	1.1841(2)
3.2	1.1423(3)
3.1	1.0986(5)
3	1.0531(7)

**Table 6:** Structure constant  $f_{\sigma\sigma\epsilon}$  from resummed perturbative expansion, obtained according to the methods of [41].

## 4.2 Higher fields $T'$ and $C$

The analysis of the fields  $T'$  ( $\ell = 2$ ) and  $C$  ( $\ell = 4$ ) is done along the same lines. The fit polynomials for  $\Delta_{T'}$  and  $\Delta_C$ , obtained as before, are

$$\begin{aligned} \Delta_{T'}(y) = & 6 - 0.567900778y + 0.1779633663y^2 - 0.806164966y^3 \\ & + 1.749534636y^4 - 1.684842086y^5 + 0.765011179y^6 \\ & - 0.126284231y^7, \end{aligned} \quad (\text{conformal bootstrap}), \quad (25)$$

$$\begin{aligned} \Delta_C(y) = & 6 - 1.001598184y + 0.030791232y^2 \\ & - 0.033868719y^3 + 0.041665026y^4 - 0.002907562y^5 \\ & - 0.006602770y^6, \end{aligned} \quad (\text{conformal bootstrap}). \quad (26)$$

They are shown in Fig. 18, along with the bootstrap results of [21] (red triangles) and the available epsilon-expansion series (magenta solid lines) [27, 32, 58, 59]:

$$\Delta_{T'}(y) = 6 - 0.5555556y, \quad (\text{epsilon expansion}), \quad (27)$$

$$\begin{aligned} \Delta_C(y) = & 6 - y + 0.01296296y^2 + 0.01198731y^3 \\ & - 0.006591585y^4, \end{aligned} \quad (\text{epsilon expansion}). \quad (28)$$

As shown by the cyan band, representing our fitting error, the scaling dimensions of these fields are determined with an accuracy comparable to that achieved for the low-lying  $\ell = 0$  states:  $\text{Err}(\Delta_{T'}) \approx 10^{-2}$  and  $\text{Err}(\Delta_C) \approx 3 \times 10^{-3}$ , meaning that  $\text{Err}(\Delta_{T'})/\Delta_{T'} \approx 10^{-3}$  and  $\text{Err}(\Delta_C)/\Delta_C \approx 5 \times 10^{-4}$ . Within our precision, we observe very good agreement with the results of [21] (especially for  $T'$ ). Furthermore, the unresummed epsilon expansion is again in agreement with the bootstrap results for  $d \rightarrow 4$ . Overall, the picture is consistent with the  $\ell = 0$  case discussed earlier<sup>14</sup>.

<sup>14</sup>The good behavior of the perturbative expansion for larger values of  $y \approx 0.8$  is not stressed, since it may be an artifact of the low order of the series.

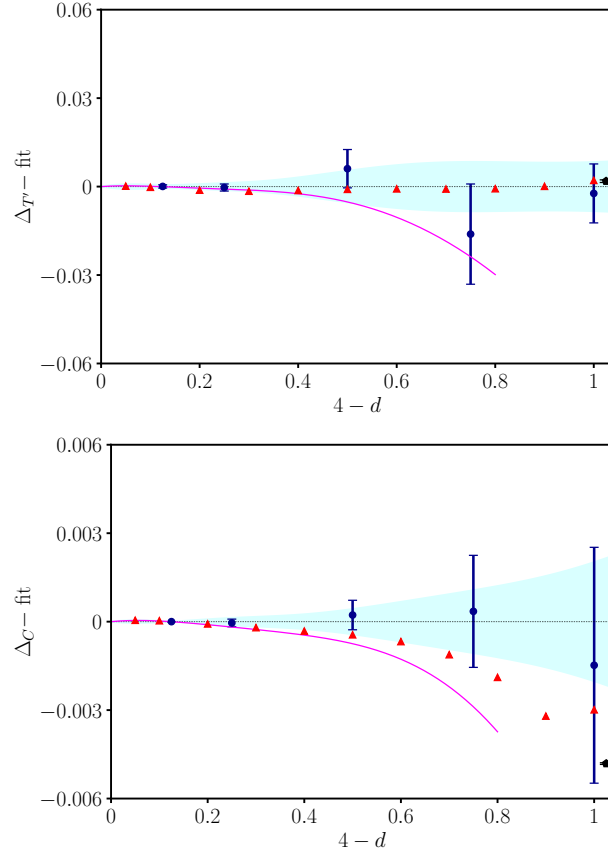


**Figure 18:** Comparison of scaling dimensions minus best fit for  $T', C$  fields: bootstrap (blue round points), navigator method [21] (triangle red points), 3-correlator bootstrap at  $d = 3$  [48] (black pentagon) and unresummed epsilon expansion [27, 32, 58, 59] (magenta solid line).

427 The corresponding structure constants are given by the polynomial fits

$$\begin{aligned} f_{\sigma\sigma T'}(y) = & 0.026278214y - 0.012019512y^2 - 0.016779681y^3 \\ & + 0.025762223y^4 - 0.018571573y^5 + 0.006902659y^6 \\ & - 0.001000504y^7, \end{aligned} \quad (\text{conformal bootstrap}), \quad (29)$$

$$\begin{aligned} f_{\sigma\sigma C}(y) = & 0.16903085 - 0.122480930y + 0.077087613y^2 - 0.591032947y^3 \\ & + 1.331591787y^4 - 1.231373513y^5 + 0.512308476y^6 \\ & - 0.079520247y^7, \end{aligned} \quad (\text{conformal bootstrap}). \quad (30)$$

428 They can be compared to the available epsilon expansions [27, 32, 58–60]:

$$f_{\sigma\sigma T'}(y) = 0.02635231y - 0.013176155y^2, \quad (\text{epsilon expansion}), \quad (31)$$

$$\begin{aligned} f_{\sigma\sigma C}(y) = & 0.16903085 - 0.12244675y + 0.02131741y^2 \\ & + 0.002168567y^3 - 0.0019760553y^4, \end{aligned} \quad (\text{epsilon expansion}). \quad (32)$$

429 The comparison is shown in Fig. 19. Also in this case we observe good agreement between the  
430 conformal bootstrap polynomials and the epsilon expansion series up to  $O(y^3)$  terms.

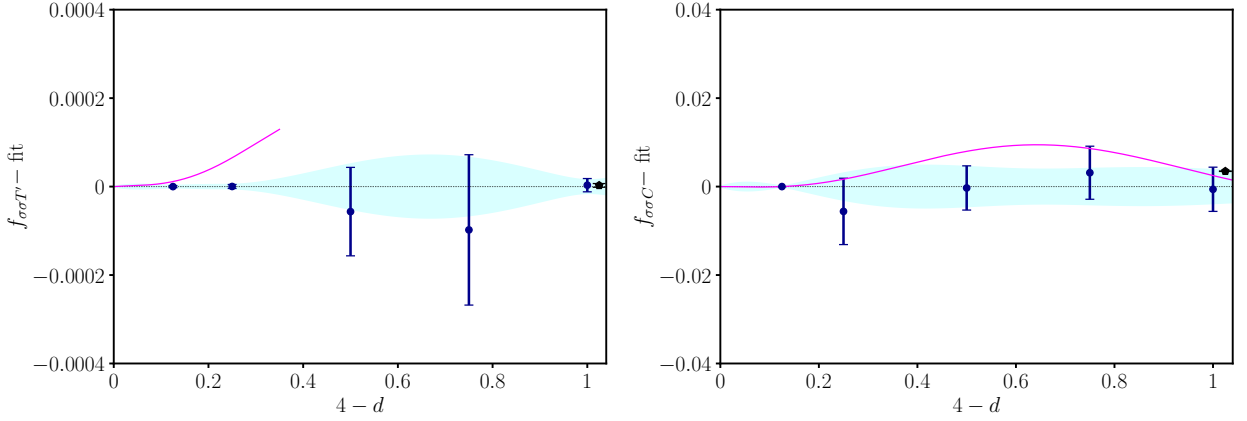


**Figure 19:** Behavior of structure constants  $f_{\sigma\sigma T'}$  and  $f_{\sigma\sigma C}$  (round blue points) compared with 3-correlator bootstrap at  $d = 3$  [48] (black pentagon) and epsilon expansion (magenta solid line) [58, 59].

### 4.3 Subleading fields $\epsilon''$ and $C'$

The numerical 1-correlator bootstrap approach used in this paper is known to have a limited precision for states higher up in the conformal spectrum, in particular for our approximation to 190 components of the truncated bootstrap equations. In this section, we show that our identification of  $\epsilon''$  ( $\ell = 0$ ) and  $C'$  ( $\ell = 4$ ) has some problems, especially for  $d \rightarrow 4$ . We explain these difficulties by using the epsilon expansion for conformal dimensions and structure constants, as well as the 3-correlator bootstrap data [21] in varying dimensions, which are definitely more accurate for the higher spectrum than our results. We think that these aspects are worth discussing, especially because the  $y = 4 - d$  dependence plays a crucial role.

We start our analysis from the subleading twist  $\ell = 4$  operator  $C'$ , for which we find the following best fit polynomial:

$$\begin{aligned} \Delta_{C'}(y) = & 8 - 0.827053961y - 0.055211344y^2 + 0.053430207y^3 \\ & + 0.010354264y^4 - 0.003205703y^5, \quad (\text{conformal bootstrap}). \end{aligned} \quad (33)$$

These data are shown in Fig. 20 (left part). It turns out that  $C'$  is degenerate at  $d = 4$  with another field with same dimension and spin, called  $C'_2$ . Their dimensions are known to leading order in the epsilon expansion,

$$\Delta_{C'}(y) = 8 - 1.555556y, \quad (34)$$

$$\Delta_{C'_2}(y) = 8 - 0.833333y, \quad (\text{epsilon expansion}), \quad (35)$$

and are plotted in Fig. 20 with magenta dashed and solid lines, respectively. Near these lines, the navigator bootstrap results [21] are plotted with gold and red triangles.

One sees that our results start at  $d \rightarrow 4$  very close to  $C'_2$  (see first coefficient in polynomials (33) and (34)) and end up near  $C'$  at  $d = 3$ . Therefore, the state we found is a mixture of  $C'$  and  $C'_2$ : better numerical precision would be needed for disentangling the two states near  $d \rightarrow 4$ , obtained, e.g., by increasing the number of components approximating the bootstrap equations.

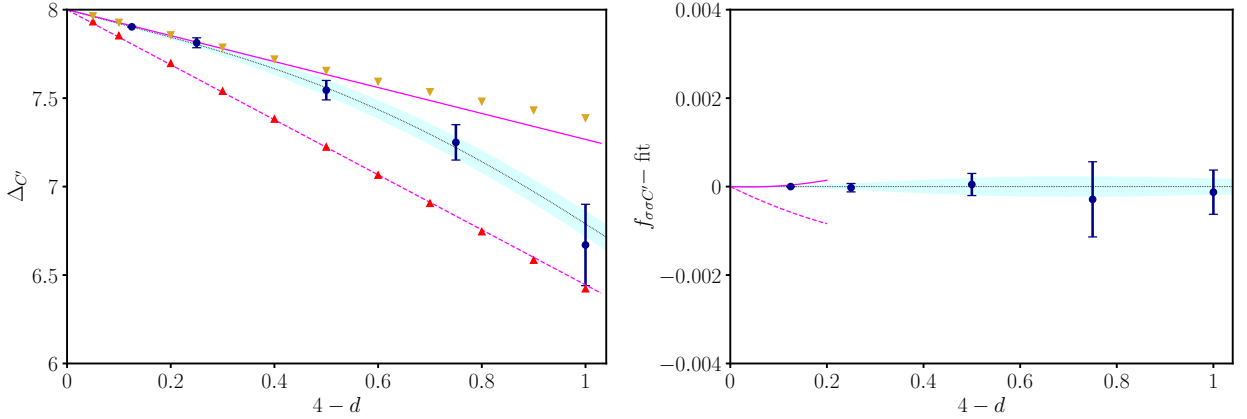


**Figure 20:** Scaling dimension and structure constant of would-be  $C'$  operator in our bootstrap spectrum (blue circles). Upward red and downward gold triangles represent navigator results for  $C'$  and  $C'_2$  [21]. The dashed and solid magenta lines are the corresponding leading-order epsilon expansion.

451 The fit of the structure constant is given by

$$f_{\sigma\sigma C'}(y) = 0.006871047y - 0.005215834y^2 - 0.003223129y^3 + 0.005087571y^4 - 0.001393464y^5, \quad (\text{conformal bootstrap}), \quad (36)$$

452 and plotted in the right part of Fig. 20. The epsilon-expansion results for  $C'$  and  $C'_2$  read,

$$f_{\sigma\sigma C'}(y) = 0.001543806y, \quad (37)$$

$$f_{\sigma\sigma C'_2}(y) = 0.006458202y, \quad (\text{epsilon expansion}), \quad (38)$$

453 and are shown as magenta dashed and solid lines on the right of Fig. 20.

454 These perturbative data show a remarkable fact: for  $d < 4$  the state of higher dimension  $C'_2$   
 455 has a larger structure constant, contrary to the standard behavior of  $f_{\sigma\sigma\mathcal{O}}$  decreasing fast with  
 456  $\Delta_{\mathcal{O}}$ . It is thus clear that, close to  $d = 4$ ,  $C'_2$  gives the dominant contribution to a putative mixed  
 457  $C'-C'_2$  state. This suggests the reason why our results with limited precision start close to  $C'_2$ . The  
 458 analysis is confirmed by the bootstrap result for the structure constant in (36): for  $d \rightarrow 4$  it fits the  
 459 perturbative behavior of  $f_{\sigma\sigma C'_2}$ , as seen in the right plot of Fig. 20. In conclusion, our subleading  
 460  $\ell = 4$  state is identified as  $C'_2$  for  $d \rightarrow 4$ , but gradually approaches  $C'$  in  $d = 3$ .

461 Another problematic identification concerns the  $\epsilon''$  field (corresponding to  $\phi^6$  in the  $\phi^4$  theory).  
 462 The best fit of bootstrap data gives

$$\Delta_{\epsilon''}(y) = 2.313321845y - 1.678645012y^2 + 0.336440006y^3 + 0.090959178y^4, \quad (\text{conformal bootstrap}), \quad (39)$$

463 while the leading epsilon-expansion result reads [24, 25, 60]:

$$\Delta_{\epsilon''}(y) = 2y - 4.759259y^2, \quad (\text{epsilon expansion}). \quad (40)$$

464 For the structure constant we find

$$f_{\sigma\sigma\epsilon''}(y) = 0.002851280y^2 - 0.003188068y^3 + 0.001218496y^4 - 0.000161879y^5, \quad (\text{conformal bootstrap}); \quad (41)$$

$$f_{\sigma\sigma\epsilon''}(y) = 0.006901444y^2, \quad (\text{epsilon expansion}). \quad (42)$$

465 It is apparent that our bootstrap results do not match the leading perturbative expansion for  $d \rightarrow 4$ .  
 466 The corresponding plots are shown in Fig. 21, where the disagreement with bootstrap results from  
 467 Ref. [21] (red triangles) is also seen.

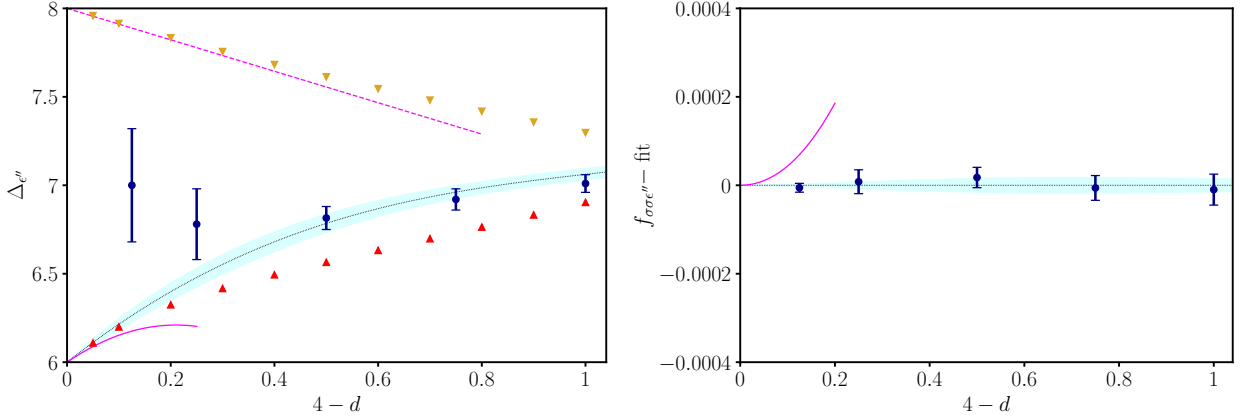


**Figure 21:** Scaling dimension and structure constant of the would-be  $\epsilon''$  operator in our bootstrap spectrum (blue circles). Upward red and downward gold triangles represent navigator results for  $\epsilon''$  and  $\epsilon'''$  [21]. The solid and dashed magenta lines are the corresponding leading-order epsilon expansion, which agree with the navigator results, but not ours.

468 Let us investigate the possibility of another mixing of states near  $d \rightarrow 4$ . In this case there is no  
 469 degenerate field with  $\epsilon''$  at  $d = 4$ . However, the next subleading one  $\epsilon''' \sim \square^2 \phi^4$  in the  $\phi^4$  theory  
 470 is present at higher dimension  $\Delta_{\epsilon'''} \leq 8$ . The epsilon expansion and navigator results for this field  
 471 are also shown in Fig. 21 (left part, gold downward triangles). We remark that a mixing of  $\epsilon''$  and  
 472  $\epsilon'''$  was shown to take place at  $d = 2.8$ , i.e., rather far from  $d = 4$  [21].

473 We suppose that the limited resolution of our data finds a state which is a mixture of  $\epsilon''$  and  $\epsilon'''$   
 474 also for  $d \rightarrow 4$ , but we cannot be certain of this. As for  $C'$  and  $C'_2$ , support for this argument could  
 475 come from a comparison of the corresponding structure constants  $f_{\sigma\sigma\epsilon''}$  and  $f_{\sigma\sigma\epsilon'''}$ . Unfortunately,  
 476 the epsilon expansion of the latter is not available, so we cannot get a definite explanation of our  
 477  $\Delta_{\epsilon''}$  data.

## 478 5 Conclusions

479 In this paper we obtained the conformal dimensions and structure constants of the critical Ising  
 480 CFT as a function of varying dimension  $4 > d \geq 3$  by using the numerical conformal bootstrap  
 481 approach.

482 Our main result is the precise determination of the anomalous dimensions of the  $\sigma, \epsilon, \epsilon'$  fields,  
 483 which are related to the Ising critical exponents  $\eta, \nu, \omega$ . Our relatively simple 1-correlator bootstrap  
 484 setup is able to compute the  $d$ -dependence of these quantities with up to one-per-thousand relative  
 485 accuracy; therefore, our findings can be used as a benchmark for future studies in non-integer  
 486 space dimension. For these low-lying states of the conformal spectrum, our results are in very good  
 487 agreement with those of more advanced 3-correlator bootstrap techniques [21, 37, 47, 48], with a  
 488 small offset included in the error estimate.

489 We presented a detailed comparison of available predictions from different methods. For  $d \rightarrow 4$ ,  
490 our results agree with those from unresummed perturbation theory. This shows two things: that  
491 non-perturbative differences, which might effect the bootstrap program or the resummed series,  
492 are negligible for  $d \rightarrow 4$ . The other non-trivial result is that both approaches agree on the same  
493 analytic continuation in dimension. A possible explanation of this correspondence is provided by  
494 the analytical bootstrap, which on one hand reproduces the epsilon expansion, and on the other  
495 hand uses the same ingredients as the numerical bootstrap.

496 For  $3 \leq d < 4$ , but away from  $d = 4$ , the bootstrap data agree very well with other results,  
497 obtained by resummation techniques of the perturbative series, Monte Carlo simulations, and other  
498 bootstrap approaches. In the whole  $4 > d \geq 3$  range we find overall consistency among the different  
499 approaches; improvements are needed by adding further terms to the perturbative series in  $d = 3$ ,  
500 as the current state of the art still shows a  $O(10^{-3})$ ,  $O(10^{-2})$  discrepancy, respectively for  $\nu$  and  
501  $\omega$ , and in general much larger error bars than bootstrap and Monte Carlo results.

502 We were able to compute bootstrap data for the conformal dimensions of higher-order fields  
503 in  $4 > d \geq 3$ , including the lowest-lying spinful fields  $T'$  ( $\ell = 2$ ) and  $C$  ( $\ell = 4$ ), with a precision  
504 comparable to that of spinless operators. The central charge and OPE coefficients of low-lying fields  
505 were obtained with even higher precision than that of the corresponding anomalous dimensions.  
506 The structure constants agree well with those of the 3-correlator bootstrap, where available (mostly  
507 in  $d = 3$ ), and with perturbation theory for  $d \rightarrow 4$ .

508 A possible future development is to improve current bootstrap results in the region  $3 > d \geq 2$ , in  
509 order to better understand how the  $d = 3$  theory approaches the  $d = 2$  Virasoro minimal model. To  
510 this aim, it is important to go beyond the lowest-lying states and precisely probe higher-dimensional  
511 and higher-spin fields. Improved 3-correlator bootstrap protocols, such as the recently proposed  
512 navigator method, may be well suited here.

## 513 Acknowledgements

514 We are grateful to C. Bonati, R. Guida, J. Henriksson, S. Kousvos, L. Maffi, R. Pisarski,  
515 M. Reehorst, S. Rychkov, M. Serone and B. Sirois for useful discussions. We thank Insitut Pas-  
516 cal for organizing the workshop “Bootstat”, where this work was initiated. CB acknowledges the  
517 support of the Italian Ministry of Education, University and Research under the project PRIN  
518 2017E44HRF, “Low dimensional quantum systems: theory, experiments and simulations”. Numer-  
519 ical computations have been performed on the *Zefiro* cluster of the Scientific Computing Center  
520 at INFN Pisa.

## 521 Appendix

## 522 A Orthogonal polynomial regression

523 Standard polynomial regression of the data set  $S \equiv \{x_i, y_i, \Delta y_i\}_{i=1}^N$  is achieved by minimizing

$$\chi^2 = \sum_{k=1}^N \left( \frac{y_k - f(x_k)}{\Delta y_k} \right)^2, \quad (43)$$

524 with respect to the parameters  $\{c_i\}_{i=0}^d$  of the fit function,

$$f_n(x) = \sum_{r=0}^n c_r x^r. \quad (44)$$

525 The degree  $n$  of the polynomial is not known a priori.

526 A smarter fit is obtained by changing the basis in which the polynomial is expressed:

$$\mathcal{B}_{\text{naive}} = \{1, x, x^2, \dots, x^d\} \rightarrow \mathcal{B}_{\text{ortho}} = \{P_0(x), P_1(x), P_2(x), \dots, P_d(x)\}, \quad (45)$$

527 where the polynomials  $P_k(x)$  (of degree  $k$ ) are chosen to be *orthogonal* on the independent variables  
528 of the dataset  $S$ , i.e.:

$$\langle P_r(x) P_s(x) \rangle_S = \frac{1}{N} \sum_{k=1}^N P_r(x_k) P_s(x_k) = k_r^2 \delta_{rs}, \quad (46)$$

529 where  $k_r$  are constants. With this choice, the fit function becomes

$$f_n(x) = \sum_{r=0}^n \alpha_r P_r(x). \quad (47)$$

530 The best fit is obtained by minimizing  $\chi^2$  in Eq. (43). The advantage of the orthogonal polynomial  
531 regression is that the coefficients  $\alpha_r$  do not depend on the  $\alpha_s$  with  $s > r$ , i.e., adding higher-degree  
532 polynomials  $r > n$  to  $f_n(x)$  does not change the value of  $\alpha_r$  with  $r \leq n$  within the statistical  
533 errors [49]. Thus, this procedure is better suited to assess the optimal degree of the polynomial.

534 The expression of the polynomials  $P_r(x)$  is known in the literature. In this work, we follow the  
535 conventions of Ref. [49]. We start by fixing the  $r = 0$  and  $r = 1$  polynomials as

$$P_0(x) = 1, \quad P_1(x) = 2(x - a_1), \quad a_1 = \frac{1}{N} \sum_{k=1}^N x_k \equiv \bar{x}. \quad (48)$$

536 Higher-order polynomials with  $r \geq 2$  are obtained through the recursive relation [49],

$$P_{r+1}(x) = 2(x - a_{r+1})P_r(x) - b_r P_{r-1}(x), \quad (49)$$

537 where the coefficients  $a_{r+1}$  and  $b_r$  are given by

$$a_{r+1} = \frac{\sum_{k=1}^N x_k P_r^2(x_k)}{\sum_{k=1}^N P_r^2(x_k)}, \quad b_r = \frac{\sum_{k=1}^N P_r^2(x_k)}{\sum_{k=1}^N P_{r-1}^2(x_k)}. \quad (50)$$

538 In this work, we find the best fitting polynomial for  $\gamma_{\mathcal{O}}$  and  $f_{\sigma\sigma\mathcal{O}}$  as a function of  $y = 4 - d$ . We  
 539 always assume their known analytic value for  $d = 4$ , for example  $\gamma_{\mathcal{O}}(d = 4) = 0$ . To enforce such  
 540 constraint, it is sufficient to use as fit function

$$h_n(x) = f_n(x) - f_n(0) = \sum_{r=1}^n \tilde{\alpha}_r [P_r(x) - P_r(0)]. \quad (51)$$

541 Finally, we reconstruct the original expansion in the naive basis by summing all equal monomials  
 542 among every  $P_r(x)$  included in the fit function:

$$h_n(x) = \sum_{r=1}^n \tilde{\alpha}_r [P_r(x) - P_r(0)] = \sum_{r=1}^n \tilde{c}_r x^r, \quad (52)$$

543 where

$$\tilde{c}_r = \sum_{l=r}^n \tilde{\alpha}_l \left. \frac{d^r P_l(x)}{dx^r} \right|_{x=0}. \quad (53)$$

544 Once the two expansions are properly matched, the coefficients obtained from orthogonal poly-  
 545 nomials agree with those obtained using a standard polynomial fit. The advantage of orthogonal  
 546 polynomials resides in their improved numerical stability, which results in an improved precision in  
 547 the computation of the  $c_i$ .

548 Finally, once the best fitting polynomial is obtained, we assign an error to our best fit function  
 549  $h_n(x)$  through standard error propagation, via the so-called parameter covariance matrix,

$$C_{ij} \equiv \text{Cov}(\tilde{\alpha}_i, \tilde{\alpha}_j). \quad (54)$$

550 Let us define  $v_i(x)$  as the gradient of the fit function with respect to the  $i^{\text{th}}$  fit parameter,

$$v_i(x) = \frac{\partial h_n(x | \vec{\tilde{\alpha}})}{\partial \tilde{\alpha}_i}. \quad (55)$$

551 The error on the best fitting polynomial is

$$\text{Err}(h_n)(x) = v^T(x) C v(x) = C_{ij} v_i(x) v_j(x). \quad (56)$$

552 The best fit of  $\gamma_{\mathcal{O}}(y)$  via orthogonal polynomial regression was done by using the `curve_fit` routine  
 553 from the standard Python library `scipy`.

## 554 B Resummation of perturbative series

### 555 B.1 Toy model example

556 In this appendix, we discuss the perturbative expansion of a toy model in dimension zero:

$$\mathcal{I}(g) \equiv \int_{-\infty}^{\infty} \frac{dx}{\sqrt{2\pi}} e^{-\frac{x^2}{2} - gx^4}. \quad (57)$$



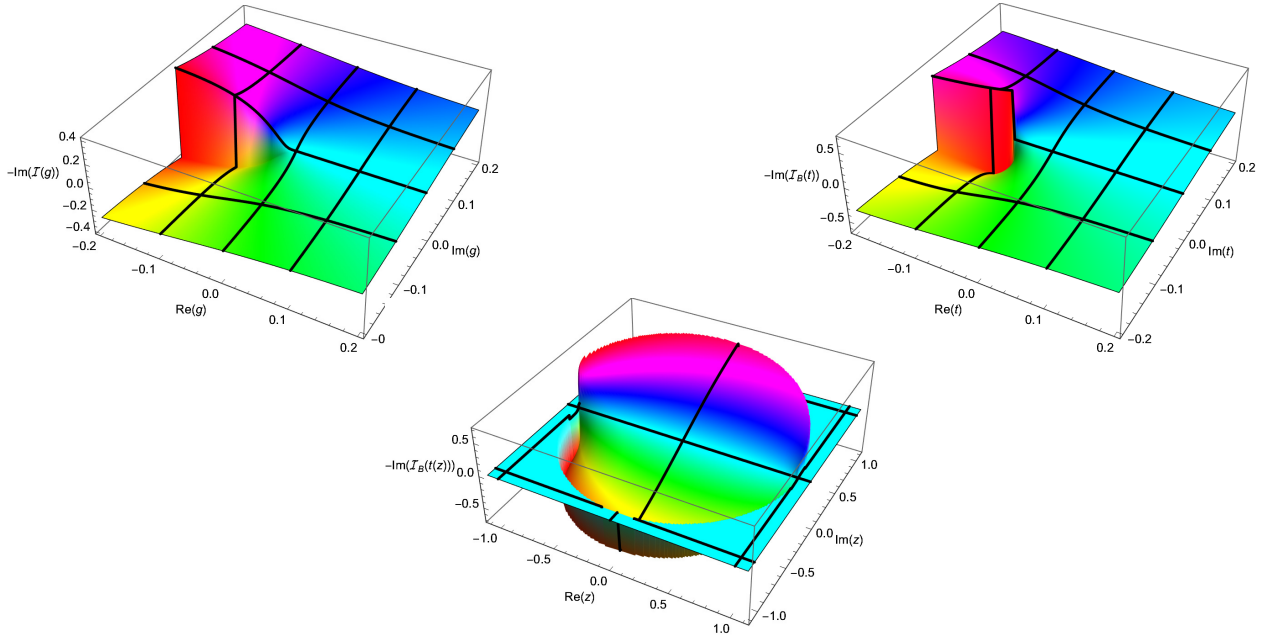


**Figure 22:** The branch cut in  $\mathcal{I}(g)$  (top left) and  $\mathcal{I}_B(t)$  (top right). While the former starts at  $g = 0$ , the latter is moved to  $g = -1/16$ . The lower plot shows  $\mathcal{I}_B(t(z))$ , which now has a branch-cut singularity at  $|z| = 1$ . (We set  $\mathcal{I}_B(t(z))$  to 0 outside the disc  $|z| \geq 1$ .)

557 Its perturbative expansion is

$$\mathcal{I}(g) = \sum_{n=0}^{\infty} a_n (-g)^n, \quad a_n = \frac{(4n)!}{2^{2n}(2n)!n!} \underset{n \rightarrow \infty}{\sim} \frac{2^{4n}}{\sqrt{2\pi n}} \times n!. \quad (58)$$

558 The analytic continuation of the integral (57) from  $\text{Re}(g) > 0$  to the full complex plane is given by  
 559 a second-kind modified Bessel  $K$ -function:

$$\mathcal{I}(g) = \frac{1}{4\sqrt{\pi g}} e^{\frac{1}{32g}} K_{\frac{1}{4}} \left( \frac{1}{32g} \right). \quad (59)$$

560 Using the asymptotic behavior of  $K_{\frac{1}{4}}(z)$  for  $z \rightarrow \infty$ , one sees that the exponential prefactor is  
 561 canceled, and the series (58) recovered. Note that  $\mathcal{I}(g)$  has a cut on the whole negative real axis,  
 562 see Fig. 22.

563 In field theory, the divergent series is analytically continued without the knowledge of its exact  
 564 expression. Let us explain the strategy on the example of integral (57). The basic idea [51] to  
 565 obtain a convergent series out of Eq. (58), is to divide each term by  $n!$ , defining the *Borel transform*  
 566  $\mathcal{I}_B(t)$  of the series. In a second step, one reconstructs the original series via an integral transform:

$$\mathcal{I}_B(t) \equiv \sum_{n=0}^{\infty} \frac{a_n}{n!} (-t)^n, \quad \mathcal{I}(g) = \int_0^{\infty} dt e^{-t} \mathcal{I}_B(tg). \quad (60)$$

567 In our example we know the analytic expression in terms of the first-kind complete elliptic integral  
 568 function

$$\mathcal{I}_B(t) = \frac{2K_{\text{elliptic}} \left( \frac{1}{2} - \frac{1}{2\sqrt{16t+1}} \right)}{\pi \sqrt[4]{16t+1}}. \quad (61)$$

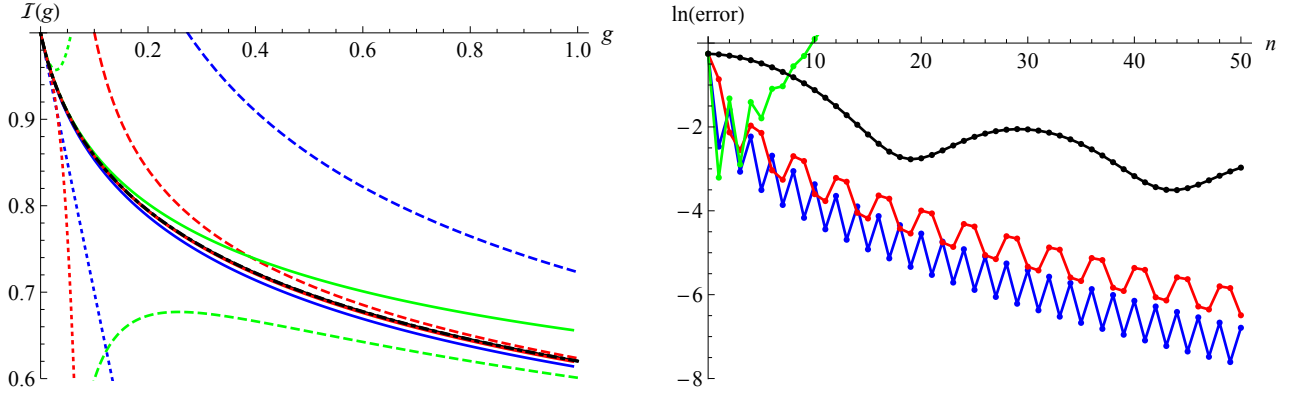


**Figure 23:** Left: function  $\mathcal{I}(g)$  (black, thick, dot-dashed) and its diverse approximations. Dotted for the series expansion at order 1 (blue), 2 (green), and 3 (red). Solid for the resummed series at the same order. Dashed for the large- $g$  expansion (same color code). Right: deviation of the resummed series (65) from the exact result (61) for  $g = 10$  as a function of  $n$ , assuming one knows  $t_{bc}$  only approximately. In blue for  $t_{bc} = -1/16$  (the exact result), in red  $t_{bc} = -1/32$  (a conservative guess), in black  $t_{bc} = -1/1000$  (much too small). Resummation with  $t_{bc} = -1/15$  (green) does not work. We see that conform to expectations, taking a too small value for  $-t_{bc}$ , the series converges more slowly, while taking a too large value of  $-t_{bc}$  the series does not converge.

569 The Borel transform  $\mathcal{I}_B(t)$  has a finite radius of convergence, denoted by  $-t_{bc}$  (equal to  $1/16$  in  
 570 our example). As a consequence, the start of the branch cut is moved from  $g = 0$  to  $t = t_{bc} < 0$ ,  
 571 see figure 22. Since the radius of convergence of  $\mathcal{I}_B(t)$  is still finite, the integral transform (60)  
 572 does not work as written. One first has to continue  $\mathcal{I}_B(t)$  to the domain  $0 \leq t < \infty$ . This can be  
 573 achieved by replacing the known truncated series via a converging Padé approximant, leading to a  
 574 *Padé-Borel resummation*.

575 A more powerful strategy is to use a conformal mapping. The most common ansatz is to assume  
 576 that at  $t = t_{bc} < 0$  a cut-singularity starts, which extends on the negative real axis to  $t = -\infty$ .  
 577 One first maps the complex plane with the expected branch cut of  $\mathcal{I}_B(t)$  onto the inside of the  
 578 unit-circle:

$$z = \frac{\sqrt{1 - t/t_{bc}} - 1}{\sqrt{1 - t/t_{bc}} + 1} \iff t = \frac{-4t_{bc}z}{(z - 1)^2}. \quad (62)$$

579 Next one constructs a series in  $z$  by expanding both sides in this variable:

$$f(z) \equiv \sum_{n=0}^{\infty} c_n z^n = \sum_{n=0}^{\infty} \frac{a_n (-t(z))^n}{n!} = \mathcal{I}_B(t(z)). \quad (63)$$

580 This series is expected to converge for  $|z| < 1$ , a fact we can check for our example (but which is  
 581 difficult to prove in general):

$$f(z) = 1 - \frac{3z}{4} + \frac{9z^2}{64} - \frac{51z^3}{256} + \frac{1353z^4}{16384} - \frac{7347z^5}{65536} + \frac{61617z^6}{1048576} + \mathcal{O}(z^7). \quad (64)$$

582 Given  $n$  terms in the original series, we know  $f(z)$  up to the same order. Using this approximation  
 583 for  $f(z)$ , we finally obtain:

$$\mathcal{I}(g) = \int_0^{\infty} dt e^{-t} \mathcal{I}_B(tg) = \frac{1}{g} \int_0^{\infty} dt e^{-t/g} \mathcal{I}_B(t) = \frac{1}{g} \int_0^1 dz t'(z) e^{-t(z)/g} f(z). \quad (65)$$

584 The result of this resummation is shown on Fig. 23. First, in black is the analytic result (59). Next  
 585 are the first three orders in several expansions, using the same color code for order 1 (blue), 2 (green),  
 586 and 3 (red): first the direct expansion in  $g$  (dotted), then in solid the resummed expansion (65).  
 587 Dashed, we show a large- $g$  expansion obtained by changing variables  $gx^4 \rightarrow y$  in the integral (57),  
 588 and then expanding the integrand in powers of  $1/\sqrt{g}$ :

$$\begin{aligned} \mathcal{I}(g) &= \frac{1}{2\sqrt{2\pi}\sqrt[4]{g}} \int_0^\infty dy \frac{e^{-\frac{\sqrt{y}}{2\sqrt{g}}-y}}{y^{\frac{3}{4}}} \\ &= \frac{1}{2\sqrt{2\pi}\sqrt[4]{g}} \left[ \Gamma\left(\frac{1}{4}\right) - \frac{2}{3} \frac{\Gamma\left(\frac{7}{4}\right)}{\sqrt{g}} + \frac{\Gamma\left(\frac{5}{4}\right)}{8g} + \mathcal{O}\left(g^{-\frac{5}{4}}\right) \right]. \end{aligned} \quad (66)$$

## 589 B.2 Details on the resummation method

590 This appendix aims at providing a “reader’s guide” to the analysis in Ref. [40], which determines  
 591 the resummed series for the  $d = 3$  critical exponents  $\eta$ ,  $\nu^{-1}$  and  $\omega$  (related, respectively, to  $\gamma_\sigma$ ,  $\gamma_\epsilon$   
 592 and  $\gamma_{\epsilon'}$ ). The same methods are used in our work, by a simple generalization to varying dimension  
 593  $4 > d \geq 3$ . This guide, together with the introduction in the main text and the example in  
 594 App. B.1, should provide enough information to follow the discussion in Ref. [40]. In particular,  
 595 we are interested in its Sec. V. Let us denote the equations in Ref. [40] by double parentheses, e.g.,  
 596 Eq. ((25)), to avoid confusion with our numbering.

597 The resummation procedure with Borel transform and conformal mapping goes along the lines  
 598 described in our Sec. 3.2 and App. B.1. The perturbative series of a critical exponent  $f(\varepsilon)$  in  
 599  $(-2\varepsilon) = D - 4$  (cf. our  $y = 4 - d$ ) is defined in Eq. ((25)) of [40]:

$$f(\varepsilon) = \sum_{k=0}^{\infty} f_k (-2\varepsilon)^k, \quad f_k \sim C_f k! a^k k^{b_f} \quad \text{as } k \rightarrow \infty. \quad (67)$$

600 With respect to our notation (cf. our Eq. (6)), the negative sign of  $a$  is included in the power of  
 601 epsilon, and the exponent of the power-law behavior earlier denoted by  $b$  is now  $b_f$ .

602 The values for the parameters  $(a, b_f)$  are given in Eq. ((26)) for the  $\lambda\phi^4$  theory with  $O(n)$   
 603 symmetry,  $n = 1$  being the case of interest, and they are determined by the known asymptotic  
 604 behavior of the beta function. With respect to the definition given here in Eq. (11), in [40] the Borel  
 605 transform is replaced by the more general Borel–Leroy transform, defined as follows (cf. Eq. ((27))  
 606 in [40]):

$$\mathcal{B}_f^b(x) = \sum_{k=0}^{\infty} \frac{f_k}{\Gamma(k+b+1)} (-x)^k, \quad (68)$$

607 where  $b$  is a free parameter. The function  $\mathcal{B}_f^b(x)$  behaves as  $\mathcal{B}_f^b(x) \sim (1+ax)^{b-b_f-1}$  around  
 608  $x = -1/a$ .

609 The function  $\mathcal{B}_f^b(x)$  is then modified in three ways in order to define the inverse transform  
 610 and improve its convergence. The first step is the conformal mapping ((29)) already described in  
 611 App. B.1, involving the known parameter  $a$ . The second step is the addition of the power-law pref-  
 612 actor in ((30)) with a second free parameter  $\lambda$ . The third step is the “homographic transformation”  
 613  $\varepsilon = h_q(\varepsilon')$  defined in ((32)) which introduces a third free parameter  $q$ .

	$d$	$\bar{b}$	$\bar{\lambda}$	$\bar{q}$
$\eta$	3.875	11	2.56	0.20
	3.75	11	2.56	0.20
	3.5	11	2.56	0.20
	3.25	11	2.56	0.20
	3	11	2.56	0.20
$\nu^{-1}$	3.875	15	1.32	0.16
	3.75	15	1.32	0.16
	3.5	15	1.32	0.16
	3.25	14	1.30	0.16
	3	13.5	1.30	0.16
$\omega$	3.875	19	0.52	0.46
	3.75	21.5	1.02	0.40
	3.5	21.5	1.02	0.40
	3.25	22	1.02	0.40
	3	22	1.02	0.40

**Table 7:** Optimal variational parameters used here in the resummation procedure for the critical exponents  $\eta$ ,  $\nu^{-1}$  and  $\omega$ , as a function of  $4 > d \geq 3$ .

614 The resummed epsilon-expansion series  $\tilde{f}(x)$  is finally obtained from the inverse Borel transform  
 615 of the modified function  $\mathcal{B}_{f \circ h_q}^{b,\lambda,\ell}$  reported in ((33)) of [40],

$$\tilde{f}(\varepsilon) = \int_0^\infty t^b e^{-t} \mathcal{B}_{f \circ h_q}^{b,\lambda,\ell} \left( \frac{2\varepsilon t}{1 - q\varepsilon} \right) dt. \quad (69)$$

616 It depends on three free parameters:  $b$ ,  $\lambda$  and  $q$  ( $\ell$  being the perturbative order considered,  $\ell = 6$   
 617 here). Let us briefly mention how these are determined.

618 The behavior of  $\tilde{f}(\varepsilon) \equiv \tilde{f}_\ell^{b,\lambda,q}(\varepsilon)$  is studied in the cubic range

$$(b, \lambda, q) \in [0, 40] \times [0, 4.5] \times [0, 0.8]. \quad (70)$$

619 The optimal values of the parameters are chosen according to the principle of “minimal sensitivity”  
 620 (w.r.t. varying the parameters) and “fastest apparent convergence” (w.r.t. increasing the perturba-  
 621 tive order by one,  $\ell - 1 \rightarrow \ell$ ). These dependences are taken into account by a proper definition of  
 622 the error function  $E_\ell^f(b, \lambda, q)$  that is given in Eq. ((36)).

623 The global minimum of the error  $\bar{E}_\ell^f = E_\ell^f(\bar{b}, \bar{\lambda}, \bar{q})$  in the cubic range (70) identifies the optimal  
 624 values  $b = \bar{b}$ ,  $\lambda = \bar{\lambda}$  and  $q = \bar{q}$ . The final estimate for the critical exponents is obtained from  
 625 the inverse Borel transform (69) with these parameters. The optimization procedure is done in-  
 626 dependently for each dimension  $d = 4 - 2\varepsilon$ . The results for  $\bar{b}$ ,  $\bar{\lambda}$  and  $\bar{q}$  are reported in Tab. 7 for  
 627 the resummations of  $\eta$ ,  $\nu^{-1}$  and  $\omega$  at the  $d$  values considered. Note the mild dependence of the  
 628 parameters on  $d$ .

629 We remark that this brief outline brushes over many fine details discussed in Ref. [40], but  
 630 which are crucial for achieving high-quality results, as well as the comparison with other methods  
 631 developed in the extensive literature. More technical information can be found in Ref. [40] and its  
 632 supplementary material, available in [arXiv:1705.06483](https://arxiv.org/abs/1705.06483).

633 The Self Consistent resummation of perturbative data used to obtain results shown in Figs. 10,  
634 11, 12, 14 and 17, instead, does not involve the optimization of free parameters introduced before.  
635 As explained in Sec. III of [41], the asymptotic behavior (67) is fitted from the perturbative series,  
636 thus finding the position of the singularity  $x = -1/a$  of the Borel transform. Such fit is done for  
637 several values of the free parameter  $\alpha$ , defined in Eq. ((44)) of [41] and analogous to  $b_f$  in (67),  
638 varied in the range  $-6 \leq \alpha < 6$  in steps of 0.2.

639 For each  $\alpha$ , the value of  $a$  obtained from the fit is used in the conformal mapping (62) ( $t_{bc} \equiv a$ )  
640 and the resulting function is Borel inverted, giving the resummed series. The best estimate of  
641 the resummed quantity with this procedure is obtained through the mean over all the values of  
642  $\alpha$  employed, while the error bars represent the maximal and minimal values obtained varying  $\alpha$ .  
643 Since only one parameter is varied, this error estimate is less reliable than that determined by the  
644 methods of Ref. [40] described earlier.

## 645 References

- 646 [1] K. G. Wilson and M. E. Fisher, “*Critical exponents in 3.99 dimensions*”, Phys. Rev. Lett. **28**  
647 (1972) 240.
- 648 [2] J. C. Le Guillou and J. Zinn-Justin, “*Accurate critical exponents for Ising like systems in*  
649 *noninteger dimensions*”, J. Phys. (Les Ulis) **48** (1987) 19.
- 650 [3] R. Guida and J. Zinn-Justin, “*Critical exponents of the N-vector model*”, J. Phys. A **31** (1998)  
651 8103.
- 652 [4] A. Pelissetto and E. Vicari, “*Critical phenomena and renormalization group theory*”, Phys.  
653 Rept. **368** (2002) 549.
- 654 [5] V. V. Prudnikov, P. V. Prudnikov and A. A. Fedorenko, “*Field-theory approach to critical*  
655 *behavior of systems with long-range correlated defects*”, Phys. Rev. B **62** (2000) 8777.
- 656 [6] C. Behan, L. Rastelli, S. Rychkov and B. Zan, “*A scaling theory for the long-range to short-*  
657 *range crossover and an infrared duality*”, J. Phys. A **50** (2017) 354002.
- 658 [7] N. Defenu, A. Trombettoni and S. Ruffo, “*Criticality and Phase Diagram of Quantum Long-*  
659 *Range O(N) models*”, Phys. Rev. B **96** (2017) 104432.
- 660 [8] A. W. W. Ludwig, “*Critical behavior of the two-dimensional random q-state Potts model by*  
661 *expansion in (q - 2)*, Nucl. Phys. B **285** (1987) 97–142.
- 662 [9] J. L. Jacobsen, P. Le Doussal, M. Picco, R. Santachiara and K. J. Wiese, “*Critical interfaces*  
663 *in the random-bond Potts model*”, Phys. Rev. Lett. **102** (2009) 070601.
- 664 [10] Z. Komargodski and D. Simmons-Duffin, “*The Random-Bond Ising Model in 2.01 and 3 Di-*  
665 *mensions*”, J. Phys. A **50** (2017) 154001.
- 666 [11] G. Parisi and N. Surlas, “*Random magnetic fields, supersymmetry, and negative dimensions*”,  
667 Phys. Rev. Lett. **43** (1979) 744.
- 668 [12] A. Kaviraj, S. Rychkov and E. Trevisani, “*Parisi–Sourlas Supersymmetry in Random Field*  
669 *Models*”, Phys. Rev. Lett. **129** (2022) 045701.

- 670 [13] K. J. Wiese, “*Theory and experiments for disordered elastic manifolds, depinning, avalanches,*  
671 *and sandpiles*”, Rep. Prog. Phys. **85** (2022) 086502.
- 672 [14] R. Rattazzi, V. S. Rychkov, E. Tonni and A. Vichi, “*Bounding scalar operator dimensions in*  
673 *4D CFT*”, JHEP **0812** (2008) 031.
- 674 [15] S. El-Showk, M. F. Paulos, D. Poland, S. Rychkov, D. Simmons-Duffin and A. Vichi, “*Solv-*  
675 *ing the 3d Ising Model with the Conformal Bootstrap II.  $c$ -Minimization and Precise Critical*  
676 *Exponents*”, J. Stat. Phys. **157** (2014) 869.
- 677 [16] D. Poland, S. Rychkov and A. Vichi, “*The Conformal Bootstrap: Theory, Numerical Tech-*  
678 *niques, and Applications*”, Rev. Mod. Phys. **91** (2019) 015002.
- 679 [17] S. El-Showk, M. Paulos, D. Poland, S. Rychkov, D. Simmons-Duffin and A. Vichi, “*Conformal*  
680 *Field Theories in Fractional Dimensions*”, Phys. Rev. Lett. **112** (2014) 141601.
- 681 [18] B. Sirois, “*Navigating through the  $O(N)$  archipelago*”, SciPost Phys. **13** (2022) no. 4, 081.
- 682 [19] C. Behan, “*PyCFTBoot: A flexible interface for the conformal bootstrap*”, Commun. Comput.  
683 Phys. **22** (2017) no. 1, 1 – 38.
- 684 [20] A. Cappelli, L. Maffi and S. Okuda, “*Critical Ising Model in Varying Dimension by Conformal*  
685 *Bootstrap*”, JHEP **01** (2019) 161.
- 686 [21] J. Henriksson, S. R. Kousvos, M. Reehorst, “*Spectrum continuity and level repulsion: the*  
687 *Ising CFT from infinitesimal to finite  $\epsilon$* ”, [arXiv:2207.10118 [hep-th]].
- 688 [22] A. A. Belavin, A. M. Polyakov and A. B. Zamolodchikov, “*Infinite Conformal Symmetry in*  
689 *Two-Dimensional Quantum Field Theory*”, Nucl. Phys. B **241** (1984) 333.
- 690 [23] P. Di Francesco, P. Mathieu and D. Senechal, “*Conformal Field Theory*”, Springer-Verlag,  
691 New York (1997).
- 692 [24] S. Rychkov and Z. M. Tan, “*The  $\epsilon$ -expansion from conformal field theory*”, J. Phys. A **48**  
693 (2015) 29FT01.
- 694 [25] F. Gliozzi, A. L. Guerrieri, A. C. Petkou and C. Wen, “*The analytic structure of conformal*  
695 *blocks and the generalized Wilson–Fisher fixed points*”, JHEP **1704** (2017) 056.
- 696 [26] L. F. Alday, “*Large Spin Perturbation Theory for Conformal Field Theories*”, Phys. Rev. Lett.  
697 **119** (2017) 111601.
- 698 [27] L. F. Alday, J. Henriksson and M. van Loon, “*Taming the  $\epsilon$ -expansion with large spin pertur-*  
699 *bation theory*”, JHEP **1807** (2018) 131.
- 700 [28] A. Bissi, A. Sinha and X. Zhou, “*Selected Topics in Analytic Conformal Bootstrap: A Guided*  
701 *Journey*”, Phys. Rept. **991** (2022), 1 – 89.
- 702 [29] T. Hartman, D. Mazac, D. Simmons-Duffin and A. Zhiboedov, “*Snowmass White Paper: The*  
703 *Analytic Conformal Bootstrap*”, [arXiv:2202.11012 [hep-th]].
- 704 [30] F. Bertucci, J. Henriksson and B. McPeak, “*Analytic bootstrap of mixed correlators in the*  
705  *$O(n)$  CFT*”, JHEP **10** (2022), 104.



- 706 [31] J. Henriksson, “*The critical  $O(N)$  CFT: Methods and conformal data*”, Phys. Rept. **1002**  
707 (2023), 1-72.
- 708 [32] J. Henriksson and M. Van Loon, “*Critical  $O(N)$  model to order  $\epsilon^4$  from analytic bootstrap*”,  
709 J. Phys. A **52** (2019) 025401.
- 710 [33] M. Hogervorst, S. Rychkov and B. C. van Rees, “*Unitarity violation at the Wilson–Fisher fixed*  
711 *point in  $4 - \epsilon$  dimensions*”, Phys. Rev. D **93** (2016) 125025.
- 712 [34] D. Simmons-Duffin, “*A Semidefinite Program Solver for the Conformal Bootstrap*”, JHEP  
713 **1506** (2015) 174.
- 714 [35] S. El-Showk and M. F. Paulos, “*Bootstrapping Conformal Field Theories with the Extremal*  
715 *Functional Method*”, Phys. Rev. Lett. **111** (2013) 241601.
- 716 [36] S. El-Showk and M. F. Paulos, “*Extremal bootstrapping: go with the flow*”, JHEP **1803** (2018)  
717 148.
- 718 [37] M. Reehorst, S. Rychkov, D. Simmons-Duffin, B. Sirois, N. Su and B. van Rees, “*Navigator*  
719 *Function for the Conformal Bootstrap*”, SciPost Phys. **11** (2021) 072.
- 720 [38] M. Kompaniets, “*Prediction of the higher-order terms based on Borel resummation with con-*  
721 *formal mapping*”, J. Phys. Conf. Ser. **762** (2016) 012075.
- 722 [39] D. V. Batkovich, K. G. Chetyrkin and M. V. Kompaniets, “*Six loop analytical calculation of*  
723 *the field anomalous dimension and the critical exponent  $\eta$  in  $O(n)$ -symmetric  $\phi^4$  model*”, Nucl.  
724 Phys. B **906** (2016) 147.
- 725 [40] M. V. Kompaniets and E. Panzer, “*Minimally subtracted six loop renormalization of*  
726  *$O(n)$ -symmetric  $\phi^4$  theory and critical exponents*”, Phys. Rev. D **96** (2017) 036016,  
727 arXiv:1705.06483.
- 728 [41] M. V. Kompaniets and K. J. Wiese, “*Fractal dimension of critical curves in the  $O(n)$ -*  
729 *symmetric  $\phi^4$  model and crossover exponent at 6-loop order: Loop-erased random walks, self-*  
730 *avoiding walks, Ising, XY, and Heisenberg models*”, Phys. Rev. E **101** (2020) 012104.
- 731 [42] M. Hasenbusch, “*Finite size scaling study of lattice models in the three-dimensional Ising*  
732 *universality class*”, Phys. Rev. B **82** (2010) 174433.
- 733 [43] A. M. Ferrenberg, J. Xu and D. P. Landau, “*Pushing the limits of monte carlo simulations for*  
734 *the three-dimensional Ising model*”, Phys. Rev. E **97** (2018) 043301.
- 735 [44] M. Hasenbusch, “*Restoring isotropy in a three-dimensional lattice model: The Ising universal-*  
736 *ity class*”, Phys. Rev. B **104** (2021) 014426.
- 737 [45] I. Balog, H. Chaté, B. Delamotte, M. Marohnic and N. Wschebor, “*Convergence of Nonpertur-*  
738 *bative Approximations to the Renormalization Group*”, Phys. Rev. Lett. **123** (2019) 240604.
- 739 [46] N. Dupuis, L. Canet, A. Eichhorn, W. Metzner, J.M. Pawłowski, M. Tissier and N. Wschebor,  
740 “*The nonperturbative functional renormalization group and its applications*”, Phys. Rep. **910**  
741 (2021) 1.
- 742 [47] F. Kos, D. Poland and D. Simmons-Duffin, “*Bootstrapping Mixed Correlators in the 3D Ising*  
743 *Model*”, JHEP **1411** (2014) 109.

- 744 [48] D. Simmons-Duffin, “*The Lightcone Bootstrap and the Spectrum of the 3d Ising CFT*”, JHEP  
745 **1703** (2017) 086.
- 746 [49] G. A. F. Seber and A. J. Lee, “*Linear Regression Analysis*” (Second ed.), John Wiley & Sons,  
747 Inc., Hoboken, New Jersey (2003).
- 748 [50] M. Reehorst, “*Rigorous bounds on irrelevant operators in the 3d Ising model CFT*”, JHEP **09**  
749 (2022) 177.
- 750 [51] J. Zinn-Justin, “*Quantum Field Theory and Critical Phenomena*” (Fourth ed.), Clarendon  
751 Press, Oxford (2002).
- 752 [52] A. N. Vasiliev, “*The field theoretic renormalization group in critical behavior theory and*  
753 *stochastic dynamics*”, Chapman & Hall/CRC, Boca Raton (2004).
- 754 [53] O. Schnetz, “*Numbers and Functions in Quantum Field Theory*”, Phys. Rev. D **97** (2018)  
755 085018.
- 756 [54] G. V. Dunne and M. Meynig, “*Instantons or renormalons? Remarks on  $\phi_{d=4}^4$  theory in the*  
757 *MS scheme*”, Phys. Rev. D **105** (2022) 025019.
- 758 [55] I. Aniceto, G. Basar and R. Schiappa, “*A Primer on Resurgent Transseries and Their Asymp-*  
759 *totics*”, Phys. Rept. **809** (2019) 1.
- 760 [56] H. Mera, T. G. Pedersen and B. K. Nikolić, “*Fast summation of divergent series and resurgent*  
761 *transseries from Meijer-G approximants*”, Phys. Rev. D **97** (2018) 105027.
- 762 [57] G. Sberveglieri, M. Serone and G. Spada, “*Renormalization scheme dependence, RG flow, and*  
763 *Borel summability in  $\phi^4$  Theories in  $d < 4$* ”, Phys. Rev. D **100** (2019) 045008.
- 764 [58] R. Gopakumar, A. Kaviraj, K. Sen and A. Sinha, “*Conformal Bootstrap in Mellin Space*”,  
765 Phys. Rev. Lett. **118** (2017) 081601.
- 766 [59] R. Gopakumar, A. Kaviraj, K. Sen and A. Sinha, “*A Mellin space approach to the conformal*  
767 *bootstrap*”, JHEP **1705** (2017) 027.
- 768 [60] S. E. Derkachov and A. N. Manashov, “*On the stability problem in the  $O(N)$  nonlinear sigma*  
769 *model*”, Phys. Rev. Lett. **79** (1997) 1423.